Research Paper

PAIN®

OPEN VIDEO

Targeting intrinsically disordered regions facilitates discovery of calcium channels 3.2 inhibitory peptides for adeno-associated virus–mediated peripheral analgesia

Seung Min Shin[a], Justas Lauzadis[b], Brandon Itson-Zoske[a], Yongsong Cai[a,c], Fan Fan[d], Gayathri K. Natarajan[a], Wai-Meng Kwok[a,e], Michelino Puopolo[b], Quinn H. Hogan[a], Hongwei Yu[a,*]

Abstract

Ample data support a prominent role of peripheral T-type calcium channels 3.2 ($Ca_V3.2$) in generating pain states. Development of primary sensory neuron-specific inhibitors of $Ca_V3.2$ channels is an opportunity for achieving effective analgesic therapeutics, but success has been elusive. Small peptides, especially those derived from natural proteins as inhibitory peptide aptamers (iPAs), can produce highly effective and selective blockade of specific nociceptive molecular pathways to reduce pain with minimal off-target effects. In this study, we report the engineering of the potent and selective iPAs of $Ca_V3.2$ from the intrinsically disordered regions (IDRs) of $Ca_V3.2$ intracellular segments. Using established prediction algorithms, we localized the IDRs in $Ca_V3.2$ protein and identified several $Ca_V3.2$iPA candidates that significantly reduced $Ca_V3.2$ current in HEK293 cells stably expressing human wide-type $Ca_V3.2$. Two prototype $Ca_V3.2$iPAs (iPA1 and iPA2) derived from the IDRs of $Ca_V3.2$ intracellular loops 2 and 3, respectively, were expressed selectively in the primary sensory neurons of dorsal root ganglia in vivo using recombinant adeno-associated virus (AAV), which produced sustained inhibition of calcium current conducted by $Ca_V3.2$/T-type channels and significantly attenuated both evoked and spontaneous pain behavior in rats with neuropathic pain after tibial nerve injury. Recordings from dissociated sensory neurons showed that AAV-mediated $Ca_V3.2$iPA expression suppressed neuronal excitability, suggesting that $Ca_V3.2$iPA treatment attenuated pain by reversal of injury-induced neuronal hypersensitivity. Collectively, our results indicate that $Ca_V3.2$iPAs are promising analgesic leads that, combined with AAV-mediated delivery in anatomically targeted sensory ganglia, have the potential to be a selective peripheral $Ca_V3.2$-targeting strategy for clinical treatment of pain.

Keywords: T-type/Cav3.2 channels, Peripheral nervous system, Dorsal root ganglia, Adeno-associated virus, Peptide aptamer, Neuropathic pain

1. Introduction

Chronic pain is a critical national health problem for which opioid treatment has numerous risks, including misuse, overdose, and addiction, highlighting the need for new analgesic targets and strategies.[85] The peripheral nervous system is a particularly accessible site for devising new pain treatments because the primary sensory neurons (PSNs) of the dorsal root ganglia (DRG) initiate nociception and have a central role in the development and maintenance of nerve injury–induced painful neuropathy.[69] T-type/calcium channels 3.2 ($Ca_V3.2$) in PSNs regulate neuronal excitability, peripheral nociceptive transduction, and excitatory neurotransmission in dorsal horn neurons and are important mediators of pain signaling.[11,26,39]

Ample data support a prominent role of peripheral $Ca_V3.2$ in pain pathology, including elevated expression and activity in inflammatory[82] and neuropathic pain,[16] diabetic peripheral neuropathic pain,[52] chemotherapy-induced peripheral neuropathy,[80] osteoarthritis pain,[76] and postsurgical pain,[40] as well as itch.[28] However, $Ca_V3.2$ is also expressed throughout the body, including endocrine, muscle, and kidney tissues, peripheral motor neurons, and pacemaker cells of the heart,[14] and efforts to date using currently available drugs targeted to $Ca_V3.2$ administered systemically have led to inadequate analgesia and significant side effects.[10] Indeed, recent multicenter, double-blind, controlled and randomized clinical trials using the established T-type channel blocker ethosuximide (Zarontin, Pfizer)[42] or the T-type Ca^{2+} channel blocker ABT-639[81,98] were

Sponsorships or competing interests that may be relevant to content are disclosed at the end of this article.

[a] Department of Anesthesiology, Medical College of Wisconsin, Milwaukee, WI, United States, [b] Department of Anesthesiology, Stony Brook University, Stony Brook, NY, United States, [c] Xi'an Jiaotong University Health Science Center, Xi'an, Shaanxi, People's Republic of China, [d] Department of Pharmacology and Toxicology, The University of Mississippi Medical Center, Jackson, MS, United States, [e] Department of Pharmacology and Toxicology, Medical College of Wisconsin, Milwaukee, WI, United States

**Corresponding author. Address: Department of Anesthesiology, Medical College of Wisconsin, Milwaukee, WI, 53226, United States. Tel.: 414-955-5745; fax: 414-955-6507. E-mail address: hyu@mcw.edu (H. Yu).*

Supplemental digital content is available for this article. Direct URL citations appear in the printed text and are provided in the HTML and PDF versions of this article on the journal's Web site (www.painjournalonline.com).

PAIN 163 (2022) 2466–2484

http://dx.doi.org/10.1097/j.pain.0000000000002650

terminated because of the high number of adverse events, as well as failure to reduce pain,[42] so novel approaches are needed.

Molecular signaling interactions are often mediated by the regions of proteins lacking a defined tertiary structure, known as intrinsically disordered regions (IDRs). These comprise a large part of the eukaryotic proteome and have been established as key facilitators of protein regulatory functionality.[86] Intrinsically disordered regions are common in integral membrane proteins, particularly in the intracellular loops (ICLs) linking transmembrane (TM) structural domains and the protein termini. These intrinsically unstructured regions often contain protein-modulating architectures that consist of multiple domains existing as short linear peptide motifs within IDRs and functioning without a stable three-dimensional structure.[20] These types of protein domains within IDRs are named intrinsically disordered domains (IDDs),[96] which are important players in multiple signaling regulations by engaging in binding to cognate sites of multiple partners and are considered new and promising drug targets.[94]

The $Ca_V3.2$ protein consists of 4 highly structured homologous TM domains, connected by ICLs and flanked by intracellular N-termini and C-termini that serve as essential molecular interfaces for $Ca_V3.2$ regulatory signaling networks.[14] Understanding of functional domains in $Ca_V3.2$ IDRs is currently limited but would be valuable in the delineation of $Ca_V3.2$ regulatory mechanisms and for future drug development. In this study, we report identification of highly disordered regions in the $Ca_V3.2$ protein and define several $Ca_V3.2$ inhibitory peptide aptamers (iPAs) that substantially reduce $Ca_V3.2$/T-type current. Adeno-associated virus (AAV)-mediated expression of these prototype $Ca_V3.2$iPAs in PSNs in vivo produces sustained T-type Ca^{2+} current inhibition and attenuates neuropathic pain behavior in rats, suggesting $Ca_V3.2$iPAs as potential analgesic leads for translational pain therapeutic development.

2. Methods

2.1. Animals

Adult male and female Sprague Dawley rats weighing 100 to 125 g body weight (Charles River Laboratories, Wilmington, MA) were used. All animal experiments were performed with the approval of the Medical College of Wisconsin Institutional Animal Care and Use Committee in accordance with the National Institutes of Health Guidelines for the Care and Use of Laboratory Animals. Animals were housed individually in a room maintained at a constant temperature (22 ± 0.5°C) and relative humidity (60 ± 15%) with an alternating 12-hour light–dark cycle. Animals were provided access to water and food ad libitum throughout the experiment, and all efforts were made to minimize suffering. All survival surgeries were completed in a sterile environment under a surgical microscope in animals anesthetized with isoflurane (2%-5%). For tissue harvest euthanasia, animals were deeply anesthetized using isoflurane, followed by decapitation with a well-maintained guillotine. The estimated numbers of animals needed were derived from our previous experience with similar experiments and the number of experiments needed to achieve a statistically significant deviation (>20% difference at $P < 0.05$) based on a power analysis.[25,87]

2.2. Computational (in silico) designs

The rat $Ca_V3.2$ full amino acid (aa) sequence was retrieved from the UniProt KB knowledge database (UniProt Knowledgebase release 2018_11). $Ca_V3.2$ protein TM domains and intracellular termini and loops were predicted by Phobius (https://www.ebi.ac.uk/Tools/pfa/phobius/).[49] The $Ca_V3.2$ protein IDRs were predicted by analyzing the full-length rat $Ca_V3.2$ sequence using DEPICTER (DisorderEd PredictIon CenTER, http://biomine.cs.vcu.edu/servers/DEPICTER/).[4] Relative IDR aa (%) of multiple ion channels was predicted using PONDR (http://www.pondr.com/cgi-bin).[88] Potential phosphorylation sites in the $Ca_V3.2$ full aa sequence were identified using Disorder Enhanced Phosphorylation Predictor (DEPP) (http://www.pondr.com/cgi-bin/depp.cgi).[88] Potentially functional peptides (IDDs) within the IDRs were further analyzed using Motifs (http://molbiol-tools.ca/Motifs.html),[36] Eukaryotic Linear Motif (ELM, http://elm.eu.org),[45] and SLiMPrints (http://bioware.ucd.ie/slimprints.html), which predict short linear motifs (SLiMs) based on strongly conserved SLiMs within IDRs.[19] Peptide structure prediction was analyzed by I-TASSER (https://zhanglab.ccmb.med.umich.edu/I-TASSER/),[73] and the IDR feature of green fluoresent protein (GFP)-iPA was predicted by the PONDR program.

2.3. Molecular cloning and adeno-associated virus constructs

To construct the AAV vector encoding a chimeric monomer GFP (hereafter referred to as GFP) $Ca_V3.2$iPA expression cassette, the DNA fragments encoding the $Ca_V3.2$iPA peptides were synthesized and subcloned into BsrG I/Sal I sites (Genscript, Piscataway, NJ) of a single-strand AAV expressing plasmid pAAV-chicken β-actin (CBA)-GFP. This generated pAAV-CBA-GFP-$Ca_V3.2$iPAs that encode the GFP-$Ca_V3.2$iPAs fusion protein downstream a chimeric intron for enhancing transcription, driven by a hybrid human cytomegalovirus (CMV) enhancer/CBA promoter, and the mRNA stabilizing Woodchuck Posttranscriptional Regulatory Element sequence was inserted downstream of the stop codon of GFP-$Ca_V3.2$iPAs and upstream of human growth hormone poly A signals. Plasmids were subsequently used in transfection experiments and in AAV vector generation. Transfection of cultured cells was performed by a standard polyethylenimine (PEI, MW 40,000, Polysciences, Inc, Warrington, PA) transfection protocol. To package AAV2/6-GFP-$Ca_V3.2$iPAs and AAV2/6-GFP-NP (a Cav3.2 N-terminal inert peptide, see further) as a control (subsequently referred to as AAV6-$Ca_V3.2$iPAs and AAV6-$Ca_V3.2$NP, respectively) for in vivo injection, AAV vectors were produced and purified in our laboratory by previously established methods.[90] This included AAV particle purification by optiprep ultracentrifugation and concentration using Centricon Plus-20 (Regenerated Cellulose 100,000 MWCO; Millipore, Billerica, MA). The AAV titer was determined by the PicoGreen (Life Technologies, Carlsbad, CA) assay, and final aliquots were kept in 1x phosphate-buffered saline (PBS) containing 5% sorbitol (Sigma-Aldrich, St. Louis, MO) and stored at −80°C. The titers (GC/mL) of AAV6-$Ca_V3.2$iPA1, 2, and 3 and AAV6-$Ca_V3.2$NP vectors were 2.45×10^{13}, 3.05×10^{13}, and 2.64×10^{13} and 2.26×10^{13}, respectively. Two lots of viral preparations were used for in vivo experiments.

2.4. Cell culture

Human embryonic kidney 293 (HEK293) cell lines stably expressing human wide-type $Ca_V3.2$ (HEK3.2), $Ca_V3.1$ (HEK3.1), and $Ca_V3.3$ (HEK3.3) (Kerafast, Boston, MA), $Ca_V2.2$ (HEK2.2, provided by Dr. Missler at Georg-August University, Germany),[21] and neuronal NG108-15 (ATCC, Manassas, VA) were cultured in Dulbecco modified Eagle medium supplemented

with glutamax, 10% fetal bovine serum (ThermoFisher, Rockford, IL), and antibiotics using standard techniques. Dissociated DRG neuronal culture for electrophysiology was performed as previously described.[59] In brief, DRG (L4 and L5) from male rats were rapidly harvested from the isoflurane-anesthetized animals and were incubated in 0.01% liberate blendzyme 2 (Roche Diagnostics, Madison, WI) for 30 minutes, followed by incubation in 0.25% trypsin and 0.125% DNase for 30 minutes, both dissolved in Dulbecco modified Eagle medium/F12 with glutaMAX (ThermoFisher). After exposure to 0.1% trypsin inhibitor and centrifugation, the pellet was gently triturated in culture medium containing Neural basal media A (ThermoFisher) and 0.5 μm glutamine. Dissociated cells were plated onto 5% laminin-coated glass coverslips (ThermoFisher), maintained at 37°C in humidified 95% air and 5% CO_2, and were studied in approximately 6 to 8 hours after harvest in electrophysiological experiments.

2.5. Electrophysiological recordings

Electrophysiological recordings were performed, as previously described with minor modifications,[25,59,76] in a blinded manner where the electrophysiologist was not aware of the treatment. Patch pipettes, ranging from 2 to 4 MΩ resistance, were formed from borosilicate glass (King Precision Glass Co, Claremont, CA) and fire polished. Recordings were made with an Axopatch 700B amplifier (Molecular Devices, Downingtown, PA). Signals were filtered at 2 kHz and sampled at 10 kHz with a Digidata 1440A digitizer and pClamp10 software (Molecular Devices, San Jose, CA). Series resistance (5-10 MΩ) was monitored before and after the recordings, and data were discarded if the resistance changed by 20%. After achieving the whole-cell recording, capacitance (Cm) and series resistance (Rs) were compensated accordingly. All experiments were performed at room temperature (approximately 22-25°C). Patch recordings were performed on the various cell lines 3 to 4 four days after transfection.

2.5.1. T-type/calcium channels 3.2 calcium channel current on cultured cell lines

Modified Tyrode solution consists of the following (in millimolar): 140 NaCl, 4 KCl, 2 $CaCl_2$, 2 $MgCl_2$, 10 D-glucose, and 10 4-(2-hydroxyethyl)-1-piperazineethanesulfonic acid (HEPES) at a pH of 7.4 with NaOH and an osmolarity of 300 mOsm. Voltage-induced currents flowing through Ca^{2+} channels were recorded using an extracellular solution containing (in mM) the following: 2 $BaCl_2$ (or $CaCl_2$), 4-aminopyridine 1, 10 HEPES, and 140 tetraethylammonium chloride (TEACl) at a pH of 7.4 and an osmolarity of 300 mOsm. Calcium channel current (I_{Ca}) recordings were elicited by 400 ms depolarizing steps ranging between −90 mV and +60 mV in 10 mV increments with 5-s intervals between steps from a holding potential of −100 mV. Measured inward current was normalized by membrane capacitance, resulting in a T-channel I_{Ca} density corrected for cell size (pA/pF). To determine the current–voltage (I–V) relationship of voltage-dependent activation, peak I_{Ca} densities during each voltage command step were fitted to a smooth curve with a Boltzmann equation: $I = G_{max}(V - E_{rev})/\{1 + \exp([V - V_{1/2}]/k)\}$, which provided the maximum conductance (G_{max}). Normalized activation curves were fitted with a Boltzmann equation: $G/G_{max} = 1/(1 + \exp[(V_{1/2} - Vm)/k)]$, where G was calculated as follows: $G = I/(Vm - Erev)$. Steady-state inactivation curves were fitted with $I/I_{max} = 1/\{1 + \exp([V - V_{1/2}]/k)\}$. In all the equations, $V_{1/2}$ denotes the half-activation and half-inactivation potentials, Vm is the membrane potential, E_{rev} is the inversion potential, k is the slope factor, G is the conductance, and I is the current at a given Vm; G_{max} and I_{max} are the maximum conductance and current, respectively.

2.5.2. Whole-cell voltage-clamp recording on dissociated dorsal root ganglia neurons (male rats)

To record voltage-activated I_{Ca} in DRG dissociated neurons, the internal pipette solution contained the following (in mM): 110 Cs-methylsulfate, 10 TEA-Cl, 1 $CaCl_2$, 1 $MgCl_2$, 10 EGTA, 10 HEPES, 4 Mg-ATP, and 0.3 Li_2-GTP at a pH of 7.2 with CsOH and an osmolarity of 296 to 300 mOsm. Small- to medium-sized PSNs (≤40 μm soma diameter) were chosen to record T-type low-voltage–activated (LVA) I_{Ca} because these are polymodal nociceptors, and most acutely dissociated small-sized and medium-sized PSNs express T currents under both basal and pathological conditions.[40,52,57] To selectively record LVA I_{Ca}, the neurons were preincubated in a Tyrode solution with 0.2 μM ω-conotoxin GVIA, 0.2 μM nisoldipine, and 0.2 μM ω-conotoxin MVIIC for at least 30 minutes. ω-conotoxin GVIA irreversibly blocks N-type I_{Ca}, and ω-conotoxin MVIIC irreversibly blocks P-/Q-type I_{Ca}. The concentrations used were saturating in preliminary experiments. Any residual high-voltage–activated (HVA) I_{Ca} after incubation of HVA calcium channel blockers was eliminated by using fluoride in the internal pipette solution.[17,59] The fluoride (F^-)-based internal solution, which was used in all experiments examining LVA I_{Ca}, contained the following (in mM): 135 tetra-methyl ammonium hydroxide, 10 EGTA, 40 HEPES, and 2 $MgCl_2$, adjusted to pH 7.2 with hydrofluoric acid. A selective and reversible T-type Ca^{2+} channel blocker, TTA-P2 (3, 5-dichloro-N-[1-(2,2-dimethyl-tetrahydropyran-4-ylmethyl)-4-fluoro-piperidin-4-ylmethyl]-benzamide, Alomone Labs, Jerusalem, Israel), was used to confirm the T-type I_{Ca}.[17] Leak currents were digitally subtracted using a P/4 leak subtraction protocol. The peak T-current was measured after subtracted from the current at the end of the depolarizing test potential to avoid contamination with residual HVA currents. Voltage protocols consisted of 100-ms depolarizing steps from a holding potential of −60 mV for HVA or 400-ms depolarizing steps from a holding potential of −90 mV for LVA to +60 mV, in 10 mV increments with 5-seconds intervals between steps.

2.5.3. Sodium channel 1.7 current ($I_{Nav1.7}$) in NG108-15 cells

Patch recordings of $I_{Nav1.7}$ were conducted in nondifferentiated NG108-15 cells (expressing unique Nav1.7 sodium channel isoform), bathed at room temperature (25°C) in modified Tyrode solution consisting of the following (in mM): 130 NaCl, 20 tetraethylammonium-Cl, 0.01 $CaCl_2$, 5 $MgCl_2$, 10 HEPES, and 5.56 mM glucose (pH 7.4) to prevent Ca^{2+} channels from becoming Na^+ conducting. The internal pipette solution consisted of the following (in mM): 10 NaCl, 130 CsCl, 5 $MgCl_2$, 5 EGTA, Na^{2+}ATP 2.5, and 10 HEPES (pH 7.2). Voltage protocols consisted of 100-ms depolarizing pulses from a holding potential of −100 or −90 mV to test potentials ranging from −80 to +40 mV, in 10 mV increments.

2.5.4. Voltage-gated potassium channel current in NG108-15 cells

Electrophysiological recordings of potassium channel current (I_{Kv}) were conducted in nondifferentiated NG108-15 cells, bathed at room temperature (25°C) in modified Tyrode solution comprising the following (in mM): 140 NaCl, 4 KCl, 2 $CaCl_2$, 2 $MgCl_2$, 10 D-

glucose, 10 HEPES at a pH of 7.4 with NaOH and an osmolarity of 300 mOsm. The recording pipette solution in all the experiments contained the following (in mM): 95 K-Gluconate, 2 KCl, 2 $MgCl_2$, 4 MgATP, 0.3 Na_2GTP, 0.2 EGTA, and 10 HEPES at a pH of 7.2 and an osmolarity of 290 mOsm. Voltage protocols consisted of 300-ms square-wave commands from a holding potential of −80 mV for I_{Kv} channels to +120 mV, in 10 mV increments with 5-second intervals between steps.

2.5.5. Whole-cell current-clamp recording on dissociated dorsal root ganglia neurons (male rats)

Whole-cell current-clamp recording of dissociated DRG neurons was performed as previously described [59,78,92] to determine the effects of AAV-mediated $Ca_V3.2$iPA1 expression on neuronal excitability. Neurons were dissociated from DRG of sham-operated rats, rats with tibial nerve injury (TNI) only, and TNI rats injected with AAV6-3.2NP or AAV6-$Ca_V3.2$iPA1 at 6 weeks after TNI and 6 weeks after vector injection (n = 5 rats per group). Selected neurons were small-sized and medium-sized (≤40 μm in diameter) and exhibited clear GFP expression in the AAV6-3.2NP or AAV6-$Ca_V3.2$iPA1 group. For whole-cell current-clamp, patch electrodes had a resistance of 0.7 to 1.5 MΩ when filled with the pipette solution, which contained the following (in mM): 140 K-gluconate, 5 KCl, 2 $MgCl_2$, 0.2 EGTA, 10 HEPES, 4 Mg-ATP, 0.3 Na^{2+}-GTP, and 10 Na2-phosphocreatine at a pH of 7.2 with KOH and an osmolarity of 296 to 300 mOsm. The extracellular solution contained the following (in mM): 140 NaCl, 4 KCl, 2 $CaCl_2$, 2 $MgCl_2$, 10 D-glucose, and 10 HEPES at a pH of 7.4 with NaOH and an osmolarity of 300 mOsm. Whole-cell configuration was obtained in voltage-clamp mode before proceeding to the current-clamp recording mode. The membrane input resistance was calculated by dividing the end amplitude of steady-state hyperpolarizing voltage deflection by the injected current.[40] Action potentials (APs) were generated by injection of a series of current pulses (100-1000 pA in steps of 100 pA, 250 ms). The baseline (BL) potential had been recorded for 20 ms before the stimulus pulses were injected into the neurons. We defined the resting membrane potential (RMP) as the mean value of the 20- ms prestimulus potential in the first trial and the AP rheobase as the minimum current required to evoke the first AP. Given the knowledge that nerve injury induces high RMP and low rheobase in DRG neurons,[12] the neurons with stable RMP more negative than −40 mV and overshooting APs (>80 mV RMP to peak) were used for additional data collection. Excitability was characterized by determining the rheobase, defined as the minimum current necessary to achieve threshold AP firing, and the AP firing frequency elicited in response to 250 ms depolarizing current injections of progressively larger amperage in 0.1 nA increments, administered at 5-second intervals.

2.6. Measurement of cytoplasmic Ca^{2+} concentration (male rats)

Measurement of cytoplasmic Ca^{2+} concentration ($[Ca^{2+}]_c$) was performed following our previously published protocols.[59,77] In brief, DRG neurons plated on coverslips were exposed to Fura-2-AM (5 μM) at room temperature in a solution that contained 2% bovine albumin to aid dispersion of the fluorophore. After 30 minutes, coverslips were washed 3 times with regular Tyrode solution containing the following (in mM): 140 NaCl, 4 KCl, 2 CaCl2, 10 glucose, 2 MgCl2, and 10 HEPES, with an osmolarity of 297 to 300 mOsm and pH 7.4, given 30 minutes for de-esterification, and mounted in the recording chamber. Neurons were first examined under bright-field illumination, and those showing signs of lysis, crenulation, or superimposed glial cells were excluded. For $[Ca^{2+}]_c$ recording, the fluorophore was excited alternately with 340 nm and 380 nm wavelength illumination (150 W Xenon, Lambda DG-4, Sutter, Novato, CA), and images were acquired at 510 nm using a cooled 12-bit digital camera (Coolsnapfx; Photometrics, Tucson, AZ) and inverted microscope (Diaphot 200; Nikon Instruments, Melville, NY) through a 20× objective. Recordings from each neuron were obtained as separate regions (MetaFluor, Molecular Devices) at a rate of 3 Hz. After background subtraction, the fluorescence ratio R for individual neurons was determined as the intensity of emission during 340 nm excitation (I_{340}) divided by I_{380}, on a pixel-by-pixel basis. Transient changes in $[Ca^{2+}]_c$ were generated by depolarization produced by microperfusion application of K^+ (50 mM) for 0.3 seconds, which, as previously shown, selectively activates T-channel specific.[59]

2.7. Microinjection of adeno-associated virus vectors into dorsal root ganglia

Adeno-associated virus vector solution was microinjected into the right lumbar (L)4 and L5 DRG using previously described techniques.[24] In brief, the surgically exposed intervertebral foramen was slightly enlarged by removal of laminar bone. Injection was performed through a micropipette that was advanced approximately 100 μm into the ganglion. Rats received L4 and L5 DRG injections of either AAV6-Cav3.2iPA or AAV6-Cav3.2NP (one vector per rat), consisting of 2 μL with adjusted titers containing a total of 2.0×10^{10} genome viral particles for each DRG. Injection was performed over a 5-minute period using a microprocessor-controlled injector (Nanoliter 2000; World Precision Instruments, Sarasota, FL). Removal of the pipette was delayed for an additional 5 minutes to minimize the extrusion of the injectate. After the injection and closure of overlying muscle and skin, the animals were returned to their housing where they remained as the designed experiments required.

2.8. Animal pain model and behavior testing (male and female rats)

2.8.1. Tibial nerve injury

To model clinical traumatic painful peripheral neuropathy, we performed TNI, an established model of neuropathic pain after peripheral nerve injury.[87] Animals were anesthetized using isoflurane at 4% for induction and 2% for maintenance. Under anesthesia, the right sciatic nerve was exposed under aseptic surgical conditions by blunt dissection of the femoral biceps muscle. The sciatic nerve and its 3 branches (sural, common peroneal, and tibial nerves) were isolated. The tibial nerve was then tightly ligated and transected distal to the ligation. The overlying muscle and skin were then sutured after surgery. Sham-operated rats were subjected to all preceding procedures but without nerve ligation and transection.

2.8.2. Evoked behavior testing

Behavioral tests were conducted between 9:00 AM and 12:00 AM Experimenters were blinded to the treatment. Animals were habituated in individual test compartments for at least 1 hour before each testing. Sensory testing of the plantar skin included eliciting reflexive behaviors induced at threshold intensity by punctate mechanical stimulation (von Frey test [vF]), dynamic mechanical stimulation (brush), noxious mechanical stimulation (pin), cold

stimulation (acetone), and heat stimulation (Hargreaves test), which were performed as previously described.[24]

2.8.3. Gabapentin injection

Gabapentin (GBP, Sigma-Aldrich) was dissolved in saline immediately before injections and administered intraperitoneally (i.p.) at a volume of 0.5 to 1.0 mL (final dose of 100 mg/kg body weight). The hindpaw vF and Pin tests on the ipsilateral side were performed at 15-minute intervals for 3 hours after GBP injection.

2.8.4. Conditioned place preference

Spontaneous pain, which is a prominent feature of neuropathic pain conditions,[13] can be measured by CPP.[44] The ongoing aversiveness (ie, affective dimension of spontaneous pain) was determined by GBP-induced CPP test, as previously described[61] with minor modifications. A 3-chamber CPP apparatus was used (Med Associates, St. Albans, VT) in which 2 sliding doors separate the central chamber from the 2 side chambers that have distinct wall stripes and flooring. Animal movement and time spent in each chamber were measured using computer-interfaced infrared photobeams. The CPP procedure consisted of the following phases: (1) on the preconditioning day, rats were allowed to explore both sides of the chambers for 15 minutes, the time spent in each side was recorded, and the preferred and nonpreferred chambers were identified. Animals that showed a predetermined level of preference for 1 chamber (≥70% of total time) at this stage were excluded for further study; (2) on the conditioning days, place conditioning was conducted using a biased assignment approach to drug pairing: saline was paired with the preferred chamber in the morning, and GBP was paired with the nonpreferred chamber in the afternoon (injections were never paired with the middle grey chamber). Conditioning consisted of the following sequential steps: intraperitoneal injection and restriction of the animal within the nonpreferred chamber for 45 minutes. We used a 45-minute conditioning time based on tests that GBP maximally reduced TNI-induced mechanical hypersensitivity at 30-60 minutes after injection. Animals were conditioned for 2 days because 2-day GBP has been reported sufficient to produce CPP in rodent pain model[41,62]; and (3) for postconditioning testing, the animals were placed back into the middle grey chamber of the CPP device with free access to all chambers for 15 minutes. The difference score for each animal was calculated by subtracting the time spent in the saline-paired or GBP-paired chamber before pairing (during preconditioning) from the time spent in each chamber after pairing (postconditioning) and averaged within each group. Each rat had only a single CPP test 6 weeks after AAV injection. Positive CPP was confirmed if the animals spent significantly more time in the GBP-paired chamber when compared with the saline-paired compartment.

2.9. Immunohistochemistry

The previously described protocol was adopted.[91] In brief, the formalin-fixed, paraffin-embedded tissue sections were deparaffinized, hydrated, and treated by heat-induced antigen epitope retrieval in 10 mM citrate buffer at a pH of 6.0. Nonspecific binding was reduced by incubating the sections for 30 minutes with a solution of 5% bovine serum albumin in PBS and 0.05% Tween20 solution. Samples were first immunolabeled with the selected primary antibodies: GFP (1:200), $Ca_V3.2$ (1:200), Glial fibrillary acidic protein (GFAP, 1:1000), NKA1α (1:600), calcitonin gene–related peptide (1:200), IB4 1.0 μg/mL, and phosphorylated calcium/calmodulin-dependent protein kinase II (pCaMKII, 1:4000), all previously described,[76,92,93] in a humid atmosphere overnight at 4°C. All antibodies were diluted in PBS and 0.05% Tween20 solution, containing 0.05% Triton X-100 and 5% bovine serum albumin. Normal immunoglobulin G (IgG) from the same species as the first antibody was replaced for the first antibody as the negative controls. The appropriate fluorophore-conjugated (Alexa 488 or Alexa 594, 1:2000) secondary antibodies (Jackson ImmunoResearch, West Grove, PA) were used to reveal immune complexes. Afterward, the sections were rinsed for 10 minutes in PBS and either processed for a colabeling of primary and secondary antibodies or coverslipped under Shur/Mount mounting medium (ThermoFisher). To avoid false-positive results attributable to cross-binding in double-label combinations, each primary antibody raised in a different species was used. To stain nuclei, 1.0 μg/mL Hoechst33342 (Hoechst, ThermoFisher) was added to the secondary antibody mixture. The immunostaining was examined, and images were captured using a Nikon TE2000-S fluorescence microscope (El Segundo, CA) with filters suitable for selectively detecting green and red fluorescence using a QuantiFire digital camera (Optronics, Ontario, NY). For double labelling colocalization, images from the same specimen but showing different antigen signals were overlaid by digitally merging the captured images. For measurement and quantification of immunostaining, positive marker antibody immunostainings were defined as the cells with fluorescence intensity greater than average background fluorescence and 2 SDs of the cells in an adjacent section in the same slide of a negative control (the first antibody omitted) under identical acquisition parameters ($n = 10$ for different markers), identified by Hoechst counterstain at a different wavelength.

2.10. Immunoblot

Cell lysates from cultured cell lines and DRG tissue (male rats) lysates from pooled L4/L5 DRG were prepared using 1× radioimmunoprecipitation assay buffer (RIPA) ice-cold buffer (20 mm Tris-HCl pH 7.4, 150 mm NaCl, 1% Nonidet P-40, 1% sodium deoxycholate, 0.1% SDS, with 0.1% Triton X100 and protease inhibitor cocktail) and rotated at 4°C for 1 hour before the supernatant was extracted by centrifugation at 12,000*g* at 4°C for 5 minutes. To examine the subcellular localization of $Ca_V3.2$, NG108-15 cells or DRG tissue was homogenized and fractionated to obtain plasma membrane, cytosolic fractions, and nuclear fractions using the ProteoExtract Subcellular Proteome Extraction Kit (Millipore), according to the manufacturer's instructions. Protein concentration was determined using Pierce BCA kit (ThermoFisher). Equivalent protein samples were size-separated using 10% or 4% to 20% sodium dodecyl sulfate–polyacrylamide gel electrophoresis (SDS-PAGE) gels (Bio-Rad, Hercules, CA), transferred to Immun-Blot PVDF membranes (Bio-Rad), and blocked for 1 hour in 5% skim milk. The transferred polyvinylidene difluoride (PVDF) membranes were subsequently incubated overnight at 4°C with appropriate antibodies (1:1000 for GFP, 1:1000 for Cav3.2, 1:1000 for GFAP, and 1:5000 for GAPDH). Immunoreactive proteins were detected by Pierce-enhanced chemiluminescence (ThermoFisher) on a ChemiDoc Imaging system (Bio-Rad) after incubation for 1 hour with HRP-conjugated second antibodies (1:5000, Bio-Rad). The densitometry of bands of interests was analyzed using ImageJ v.1.46. Ratios of the band density of the target proteins to GAPDH band density were calculated and the fold changes of target proteins in the experimental samples compared with those from the control samples.

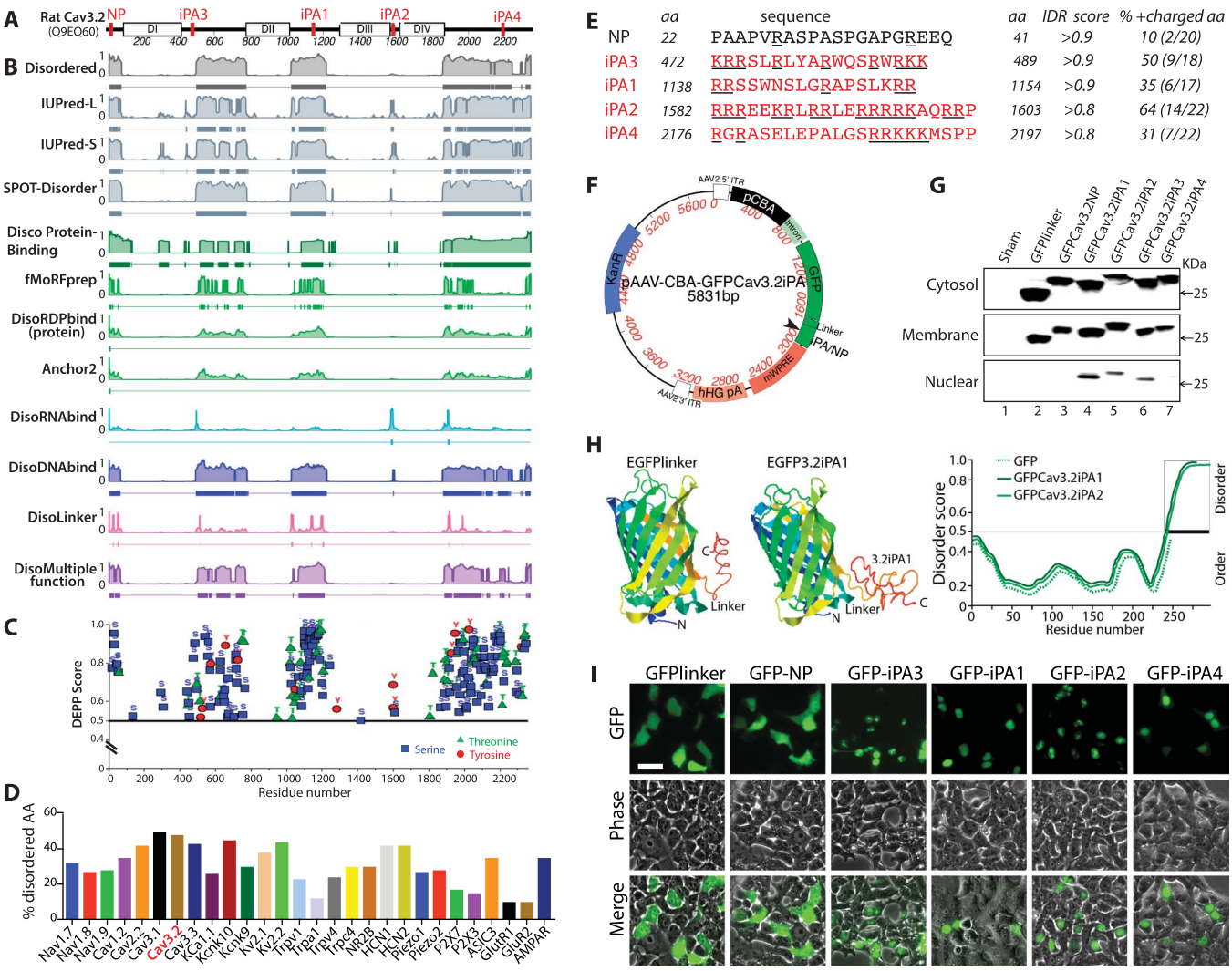

Figure 1. In silico prediction of $Ca_V3.2$-IDRs and design of candidate $Ca_V3.2$iPAs. (A) Diagram of full length of $Ca_V3.2$ protein, with white boxes labeled DI-DIV of $Ca_V3.2$ TM domain I to IV and the red bars within the sequences showing the position of the predicted iPAs. (B) IDRs are predicted by DEPICTER,[4] a prediction algorithm that aggregates results from the multiple servers (IUPred-L and IUPred-S: Prediction of Intrinsically Unstructured Proteins. SPOT-Disorder-Single: Accurate Single-Sequence Prediction of Protein Intrinsic Disorder. Disco Protein Binding: Prediction of IDR Protein Binding. fMoRFpred: Fast Molecular Recognition Feature predictor. DisoRDPbind: Predictor of disorder-mediated RNA, DNA, and protein binding regions. Anchor 2: Potential binding sites in disordered regions. DiscoRNA(DNA) Bind: Prediction of Potential RNA (DNA) binding regions. Disordered: Flexible Linker predictor. DiscoMultipleFunction: Annotations of disordered multifunctional residues), with each algorithm indicated on the left side. The top graph labeled Disordered is a consensus of others for disordered residues. (C) the phosphorylation sites (serine, threonine, and tyrosine) predicted by DEPP (disorder-enhanced phosphorylation prediction). (D) Composition of disordered amino acid in $Ca_V3.2$, compared with a number of nociception-related ion channels. (E) Five potential iPAs with their aa sequence, position in $Ca_V3.2$, IDR scores, and percentage of polybasic aa. (F) A map showing each component of an AAV plasmid coding GFP-iPA fusion with a filled black arrow pointing to iPAs or NP. (G) GFP western blots of each designed construct after transfection to HEK cells, as indicated. (H) The crystal structure analysis of GFP-linker (left) and GFP3.2iPA1 (middle) by I-TASSER and prediction of disordered scores of GFP-3.2iPA1 and 2 (right). (I) Images (GFP, top; phase, middle; and merged pictures, bottom) show cellular localization of each construct as indicated after transfection to HEK cells, scale bar: 25 μm for all. aa, amino acid; AAV, adeno-associated virus; $Ca_V3.2$, calcium channels 3.2; DEPP, disorder-enhanced phosphorylation predictor; IDR, intrinsically disordered region; iPA, inhibitory peptide aptamer; TM, transmembrane.

2.11. Statistical analyses

Statistical analysis was performed with GraphPad PRISM 9 (GraphPad Software, San Diego, CA). Behavioral changes compared with pretreatment BL, and between groups for von Frey and heat measurements, were generated using the repeated measures two-way analysis of variance and Tukey post hoc for within-group analysis and Bonferroni test for between groups. Pin and cold tests produce discrete numerical data without normal distributions, so conservative nonparametric analysis was performed by the Friedman tests and Dunn post hoc analysis. For comparisons between groups, in the pilot in vivo testing of simultaneous TNI operation and AAV injection, the effects of vector injection were characterized by area under the curve (AUC) analysis; in the treatment protocol of established pain, the measures immediately before AAV injection at the 14th day post TNI were used as the treatment BL (tBL) for calculating treatment AUC (tAUC). Calculated AUC and tAUC were compared between vectors by the Student *t* test for von Frey and heat and by the Mann-Whitney *U* test for brush, pin, and cold. Differences in the electrophysiological and immunoblot experiments were compared with the 1-way analysis of variance, 2-tailed unpaired *t* test, or Mann-Whitney test, where appropriate. Results were reported as mean and SD of the mean (SEM). Significant differences for values were reported using asterisks *, **, and ***, denoting $P < 0.05$, <0.01, and <0.001, respectively. Exact *P* values for all

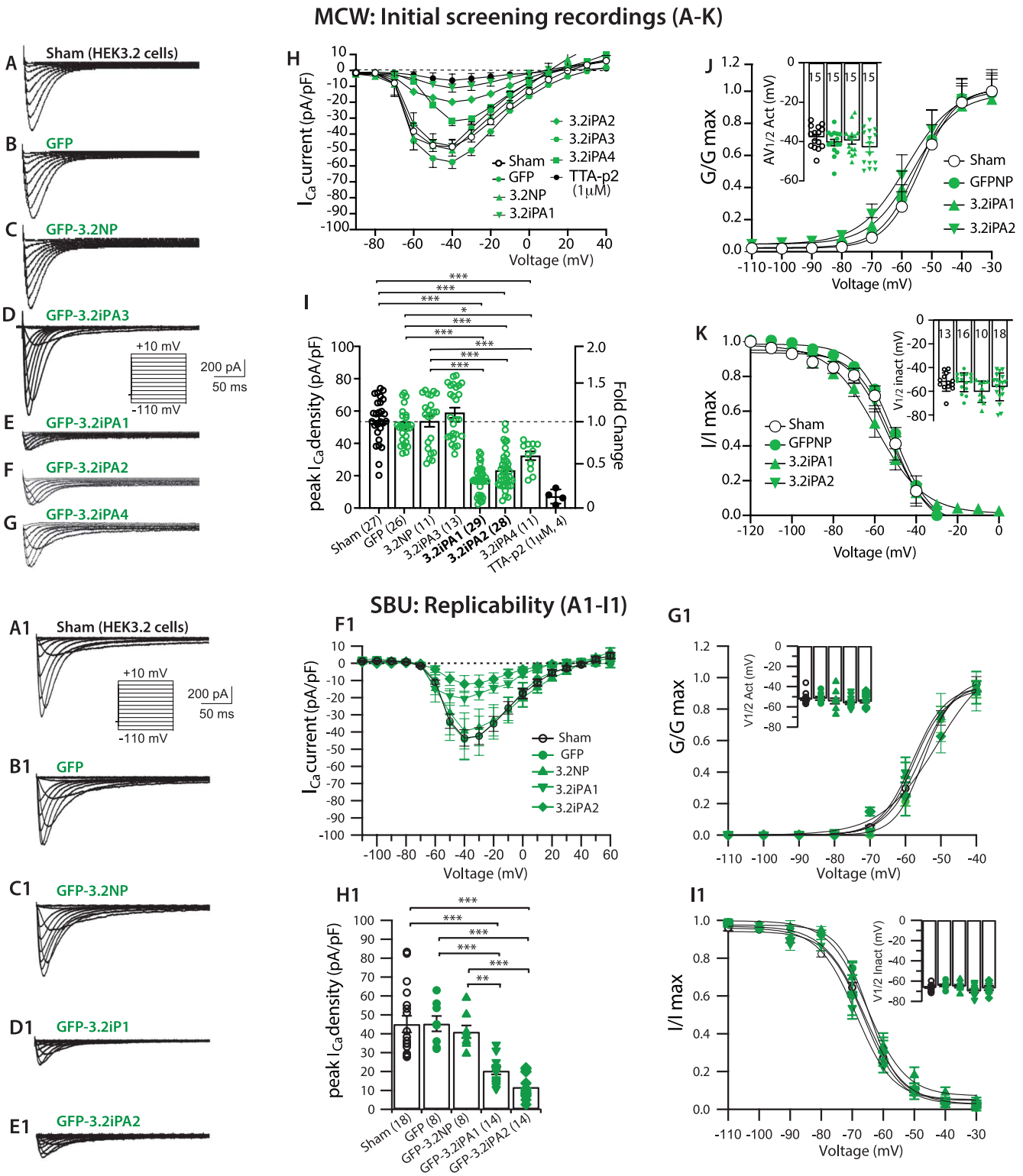

Figure 2. Inhibition of $I_{Ca3.2}$ of HEK3.2 cells by $Ca_V3.2$iPA candidates. Shown are results of functional testing of 3.2iPAs in block of $I_{Ca3.2}$ in HEK3.2 cells. In initial screening recordings: Representative Ba^{2+} current traces elicited by whole-cell voltage-clamp recording for sham-HEK3.2 cells (A) or HEK3.2 cells transfected with plasmids coding GFP (B), 3.2NP (C), 3.2iPA3 (D), 3.2iPA1 (E), 3.2iPA2 (F), and 3.2iPA4 (G), respectively (insets: recording protocol and current/time scales). Comparison of the mean peak current density–voltage (I/V) relationship from different constructs (H) and quantitative analysis of averaged peak $I_{Ca3.2}$ density as indicated (I); $^*P < 0.05$ and $^{***}P < 0.001$, 1-way ANOVA and Tukey post hoc test. No effects of expression of 3.2iPA1 and 3.2iPA2 were observed on steady-state activation (J, inset: V_{50} activation) and inactivation (K, inset: V_{50} inactivation), compared with sham-transfected and 3.2NP-transfected cells. In replicability tests from an independent external institute: $I_{Ca3.2}$ was elicited from −110 to +60 mV in 10 mV increments. The external solution was in mM: 151 TEA-Cl, 2 $CaCl_2$, 1 $MgCl_2$, 10 HEPES, and 13 Glucose, pH = 7.4. The internal solution was in mM: 125 CsCl, 10 NaCl, 1 $MgCl_2$, 10 EGTA, and 10 HEPES, pH = 7.2. Representative $I_{Ca3.2}$ recorded from sham HEK3.2 cells (A1) and from HEK3.2 cells transfected with plasmid containing GFP (B1), 3.2NP (C1), 3.2iPA1 (D1), and 3.2iPA2 (E1) (insets: recording protocol and current/time scales). (F1) I/V curves for $I_{Ca3.2}$ recorded from sham, GFP, 3.2NP, 3.2iPA1, and 3.2iPA2. (H1) quantitative analysis of averaged peak $I_{Ca3.2}$ density; $^{***}P < 0.001$, 1-way ANOVA and Tukey post hoc test. 3.2iPA1 and 3.2iPA2 on steady-state activation (G1) (inset: V_{50} activation) and inactivation (I1) (inset: V_{50} inactivation), compared with sham-transfected, GFP-transfected, and 3.2NP-transfected cells. ANOVA, analysis of variance; Ca_V 3.2, calcium channels 3.2; I_{Ca}, calcium current; G/Gmax, normalized conductance; HEPES, 4-(2-hydroxyethyl)-1-piperazineethanesulfonic acid; iPA, inhibitory peptide aptamer; I/Imax; normalized current; MCW, Medical College of Wisconsin; SBU, Stony Brook University.

figures are provided in Suppl. Table 1 (available at http://links.lww.com/PAIN/B621). To address replicability, patch-clamp characterization of iPA effects on $I_{Ca3.2}$ of cultured HEK3.2 cells was duplicated by a separate research team at Stony Brook University. Comparable methods and reagents were used there, and plasmid and vector preparations were supplied by the Medical College of Wisconsin research group. However, apart from concurring on techniques as described in this study, no contact was maintained during the performance of the experiments and analysis. Results reported further are from the Medical College of Wisconsin group unless otherwise noted.

3. Results

3.1. In silico prediction of calcium channels 3.2 intrinsically disordered regions and design of candidate $Ca_V3.2$iPAs

To identify specific IDRs, we analyzed the full-length rat $Ca_V3.2$ protein sequence using DEPICTER, which combines 10 popular algorithms for IDRs and IDR functional predictions within the primary sequence, based on aa biophysical features for the protein's disordered ensemble.[4] This returns a score between 0 and 1 for each residue, indicating the degree to which a given residue is part of an ordered or disordered region (residues with scores >0.5 are considered as disordered). Results revealed clear order-to-disorder transitions where $Ca_V3.2$ TM domains and intracellular portions join, and scores indicate a disordered nature of $Ca_V3.2$ intracellular and terminal regions (**Figs. 1A and B**). Specifically, the most extensive IDRs are in the ICLs and C-terminus, while protein TM domains are highly ordered. Owing to their extended conformation, IDRs are more exposed to other proteins and are preferred posttranslational modification sites, including sites for methylation, ubiquitination, and especially for phosphorylation, which are not only most prevalent but also serve as critical signaling nodes.[3,37,86] Potential phosphorylation sites in $Ca_V3.2$ full-length aa sequence were identified using DEPP. Results showed that most potential phosphorylation residues (serine, threonine, and tyrosine with high DEPP scores) reside in $Ca_V3.2$ IDRs and particularly in the IDRs within the ICL1, ICL2, and C-terminus (**Fig. 1C**). $Ca_V3.2$ IDRs feature as potential protein–protein interaction (PPI) binding sites, suggesting these short linear peptides are key binding motifs and domains of the $Ca_V3.2$ regulatory signaling interactome. These observations predict that focusing on the $Ca_V3.2$ IDRs could be an avenue for identifying short peptides effective in $Ca_V3.2$ functional regulation. A comparison of the components of $Ca_V3.2$ IDRs to the IDRs in a number of known nociception-related ion channels (**Fig. 1D**) showed that $Ca_V3.2$ is particularly enriched with IDRs that can be acted upon by a diverse array of regulatory proteins.

Because of difficulty in direct experimental identification and validation of the numerous possible functional sequences within $Ca_V3.2$ IDRs, the potentially functional domains within the $Ca_V3.2$ IDRs (ie, short linear peptides defined as functional intrinsically disordered domain)[96] were further analyzed using Motifs, Eukaryotic Linear Motif, and SLiMPrints. These programs predict SLiMs based on strongly conserved primary aa sequences, followed by filtering based on the prediction scores. SLiMPrints specifically identifies the relatively overconstrained proximal groupings of residues within IDRs, indicative of putatively functional IDDs.[19,58] The enumerated motifs predicted within $Ca_V3.2$ IDRs suggest many possible functional peptides as hot-spots of functional IDDs, including proteolytic cleavage sites, ligand binding sites, posttranslational modification sites, and subcellular targeting sites. Notably, $Ca_V3.2$ IDRs contain several linear polybasic peptide (PBP) sequences composed of approximately 20 aa that are enriched with positively charged arginine (R) and lysine (K), other disordered aa, and phosphorylation sites that are clustered in ICL1-3 and C-terminus and can be considered as potential regulatory IDDs. Several previous studies report that polybasic sequences in protein IDRs are crucial in the functional regulation of proteins,[7,27] and positively charged polybasic domains can be essential for recruiting multiple signaling proteins.[71,95,97] These $Ca_V3.2$IDR PBP peptides and a 20mer non-PBP peptide from the N-terminal IDR of $Ca_V3.2$ (NP) were designed computationally and were the focus as $Ca_V3.2$iPA candidates for further testing (**Fig. 1E**). Notably, candidate $Ca_V3.2$iPA3 sequence locates within the proximal peptide of $Ca_V3.2$-ICL1 that regulates $Ca_V3.2$ gating,[54] and the $Ca_V3.2$iPA2 sequence is overlaid to a peptide in $Ca_V3.2$-ICL3 that interacts with nuclear-expressed deubiquitinating enzyme USP5.[29]

3.2. Expression of $Ca_V3.2$iPAs

To allow stable and functional occupancy of $Ca_V3.2$ channels by candidate $Ca_V3.2$iPAs, we first constructed AAV expression plasmids containing transgene expression cassettes encoding various GFP-$Ca_V3.2$iPA chimeras with which we expressed GFP-$Ca_V3.2$iPAs (3.2iPAs) by transfection. Specifically, the sequences for interchangeable peptides for testing were cloned with a linker sequence (GLRSRAQASNSAVDGTAGPGS), as we described,[92] to form a chimeric transgene in a GFP-linker-3.2iPA orientation driven by CBA promoter to generate pAAV-CBA-GFP-3.2iPA (pAAV-3.2iPA) expression plasmids in which the oligonucleotides encoding the interchangeable iPAs are inserted at the 3′ end of GFP (**Fig. 1F**). The stable expression of each construct was verified by transfection into HEK293 cells (**Figs. 1G and I**). The crystal structure analysis of GFP3.2iPA1 and GFP3.2iPA2 by I-TASSER tool shows an unfolded and extended, highly flexible structural ensemble of linker-3.2iPA1, which is compatible with a well-exposed mode to bind to targets (**Fig. 1H**, I-TASSER for other iPAs not shown).

3.3. Inhibition of calcium channels 3.2 current ($I_{Ca3.2}$) by 3.2iPAs

3.3.1. HEK stable cell lines

Whole-cell voltage-clamp recordings of $I_{Ca3.2}$ in HEK3.2 cells transfected with plasmids encoding different 3.2iPAs were performed to characterize functional inhibition of $Ca_V3.2$ channels by designed 3.2iPAs. Application of the T-type calcium channel blocker TTA-P2[17] in HEK3.2 cells reduced peak $I_{Ca3.2}$ density to approximately 5% of BL level (**Fig. 2**), consistent with T-type calcium current. Transfection followed by patch clamp results showed that 3.2iPA1, 3.2iPA2, and 3.2iPA4 produced approximately70%, 60%, and 40% reduction of peak $I_{Ca3.2}$ density, respectively. Transfection with plasmids expressing the GFPlinker, 3.2NP, and 3.2iPA3 showed no significant effects on peak $I_{Ca3.2}$ density compared with sham-transfected HEK3.2 cells. These experiments thus identified 3.2iPA1 and 3.2iPA2 as effective iPAs (>50% $I_{Ca3.2}$ inhibition). In addition, their effects on $Ca_V3.2$ biophysical properties were examined, using sham-transfected cells and 3.2NP-transfected cells as the controls. Results revealed no significant shifts of the steady-state activation and inactivation curves nor on voltage-activated half activation or half inactivation (**Fig. 2**), suggesting that 3.2iPA1 and 3.2iPA2 reduced the conduction of Ca^{2+} through $Ca_V3.2$ channels but did not change

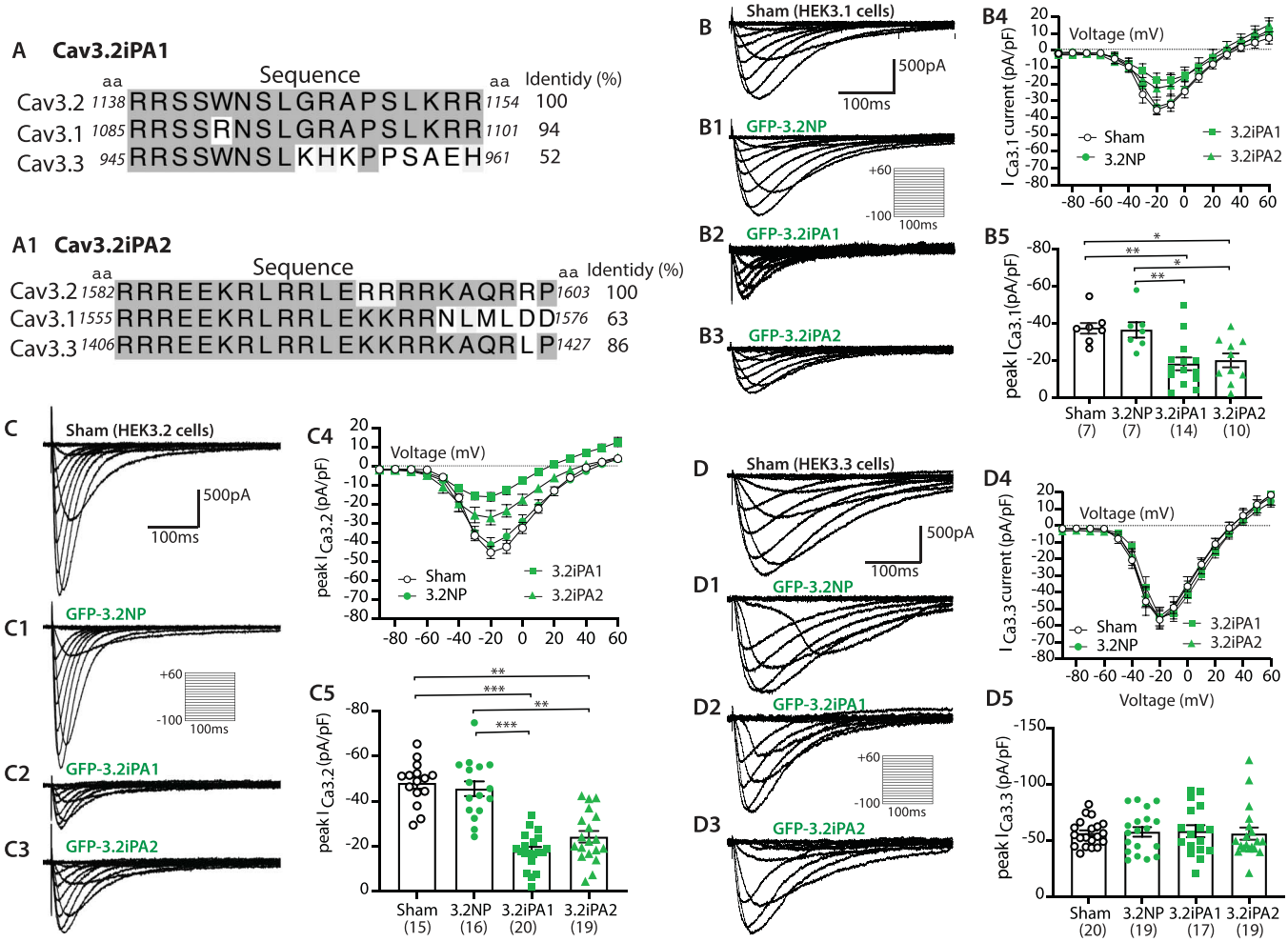

Figure 3. Inhibition of $Ca_V3.2iPA1/2$ on $Ca_V3.1$ but not $Ca_V3.3$ currents. Identification of significant aa sequence homology between 3.2iPA1/2 and the corresponding aa sequences of $Ca_V3.1$ and $Ca_V3.3$ (A, A1). Experiments compared the effects of presence of $Ca_V3.2iPA1/2$ (3.2iPA1 and 3.2iPA2) in the cells of HEK3.1, HEK3.2, and HEK3.2 on the currents of $Ca_V3.1$, $Ca_V3.2$, and $Ca_V3.3$, respectively, using sham transfection and GFP-3.2NP (3.2NP)–transfected cells as the controls. Illustrations show the I_{Ca} current traces recorded in each transfection, I/V curves, and comparison of peak I_{Ca} density from HEK3.1 (B-B5), HEK3.2 (C-C5), and HEK3.3 (D-D5) of different transfections, respectively. Insets: current/time scales and recording protocols. *, **, and *** denote $P < 0.05$, 0.01, and 0.001, respectively. One-way ANOVA and the Tukey post hoc test. aa, amino acid; ANOVA, analysis of variance; $Ca_V3.2$, calcium channels 3.2; $I_{Ca3.1}$, $Ca_V3.1$ current; $I_{Ca3.2}$, $Ca_V3.2$ current; $I_{Ca3.3}$, $Ca_V3.3$ current.

channel activation and inactivation properties. To test the replicability of these findings, the experiments testing the effects of 3.2iPA1 and 3.2iPA2 expressions on $I_{Ca3.2}$ in HEK3.2 cells were examined independently by a separate research team at a second institution (Stony Brook University), whose results were comparable with the findings generated by the Medical College of Wisconsin laboratory (**Fig. 2**). Taken together, these data confirm the efficacy of our discovery approach and indicate that signaling through PBP sequences in $Ca_V3.2$ IDRs is important in regulating $Ca_V3.2$ channel function. The findings also suggest that 3.2iPA1 and 3.2iPA2 successfully inhibit $Ca_V3.2$ channels, thereby justifying further studies of their potentials as therapeutic agents. Potent $I_{Ca3.2}$ inhibition by 3.2iPA1 was confirmed in neuronal NG108-15 cells that naturally express $Ca_V3.2$, which can be detected in subcellular locations (Suppl. Fig. 1, available at http://links.lww.com/PAIN/B621). Because the aa sequences of $Ca_V3.2iPA1$ and 2 have significant homology to the corresponding aa sequences of $Ca_V3.1$ and $Ca_V3.3$, we further tested effects of presence of $Ca_V3.2iPA1$ or 2 on $Ca_V3.1$ and $Ca_V3.3$ currents using HEK3.1 and HEK3.2 cells, compared with a set of new recordings of $Ca_V3.2$ in HEK3.2 cells. Of interest, both $Ca_V3.2iPA1$ and 2 significantly inhibit $Ca_V3.1$ current but not $Ca_V3.3$ current (**Fig. 3**). These results suggest inhibitive effects of $Ca_V3.2iPA1/2$ on fast activation/inactivation T-type channel ($Ca_V3.2$ and $Ca_V3.1$) but not on slower activation/inactivation $Ca_V3.3$, a similar biological phenomenon described in a previous report.[54]

3.4. No effects of $Ca_V3.2iPAs$ on sodium channel 1.7 and voltage-gated potassium channels (VGKCs, I_{Kv})

The LVA calcium channel can interact with big conductance (BK, KCa1.1) potassium channels, enabling KCa1.1 activation,[70] and may also affect sodium channels.[30] T-type calcium channel specificity of 3.2iPA1 and 3.2iPA2 action was therefore further examined by using neuronal NG108-15 cells that naturally express VGKCs. Interaction with the $Na_V1.7$ current was examined as well because it is a key element in pain perception.[1] Whole-cell patch-clamp recordings showed that transfection of 3.2iPA1 and 3.2iPA2 have no effects on the $I_{Na1.7}$ and the I_{Kv} compared with NG108-15 sham-transfected cells or NG108-15 cells transfected with plasmids encoding GFP or 3.2NP (**Figs. 4A and B**).

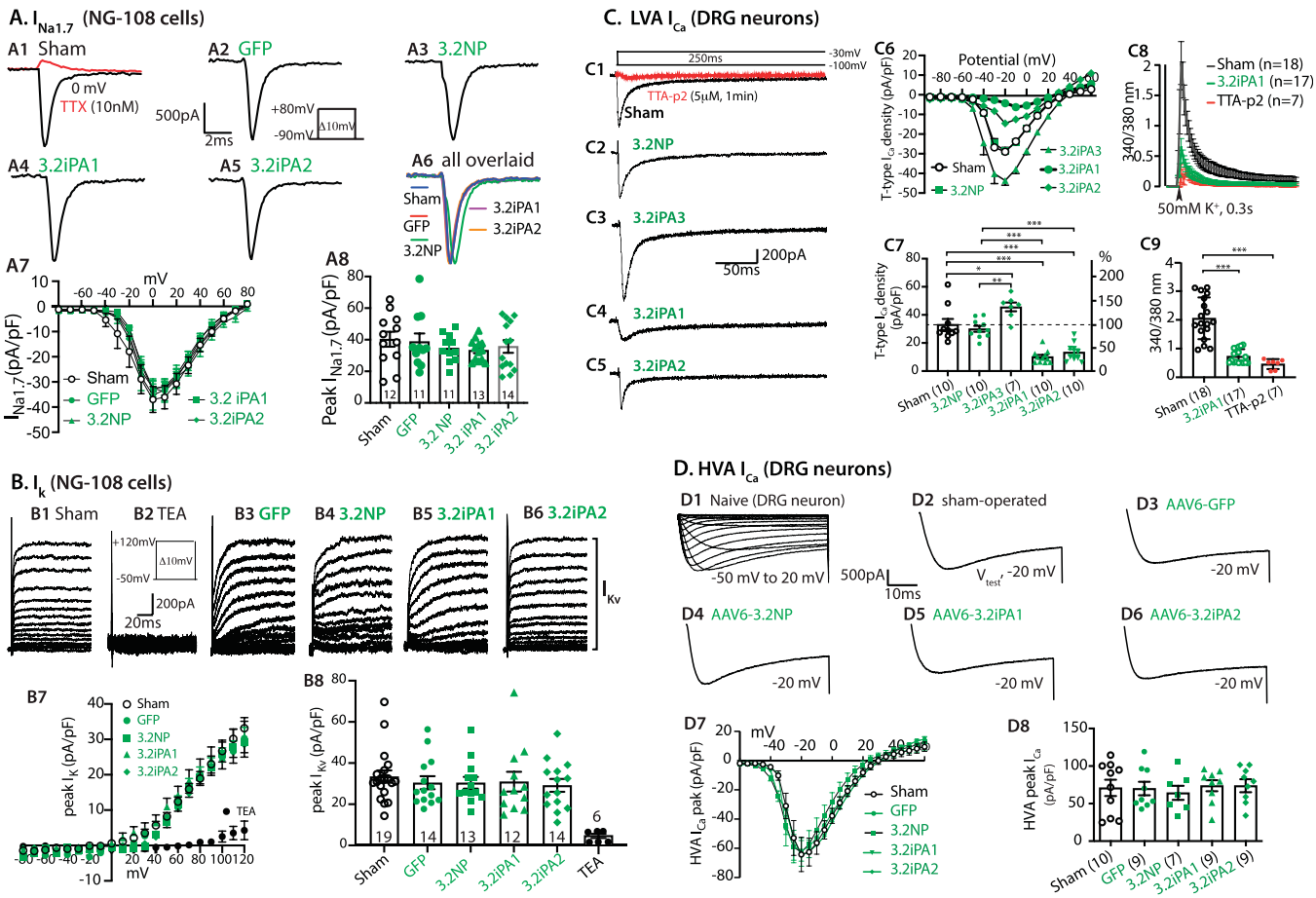

Figure 4. $Ca_V3.2$iPAs on $I_{Na1.7}$, potassium channel current, low-voltage–activated calcium channel current, and high-voltage–activated I_{Ca}. (A) Representative $I_{Na1.7}$ (single traces at 0 mV) of sham-NG108 cells showing the $I_{Na1.7}$ blocked by 10 nM of TTX in bath solution or NG108 cells transfected with GFP, 3.2NP, 3.2iPA1, 3.2iPA2, and the merged $I_{Na1.7}$ of A-E shown in (A1-A6). Insets: recording protocol and current/time scales. $I_{Na1.7}$ density–voltage (I/V) relationship from different constructs (A7) and quantitative analysis of averaged peak $I_{Na1.7}$ density (A8); $P > 0.05$, one-way ANOVA and Tukey post hoc test. (B) Representative I_{Kv} of sham-NG108 cells showing I_{Kv} defined by outward currents blocked by tetraethylammonium (TEA, 5 mM) or NG108 cells transfected with the plasmid expressing GFP, 3.2NP, 3.2iPA1, and 3.2iPA2 (B1-B6) (insets in B: recording protocol and current/time scales). Potassium channel current density–voltage (I/V) curves (B7) and quantitative analysis of averaged peak I_{Kv} density (B8); $P > 0.05$, one-way ANOVA and Tukey post hoc test. (C) Whole-cell LVA I_{Ca} recordings on DRG-dissociated neurons 4 weeks post vector injection. (C1-C5) are typical traces of T-type I_{Ca} of neurons (20-40 μm in diameter) from a naïve rat (blocked by 5 μM TTA-P2) and rats injected with AAV-3.2NP, 3.2iPA3, 3.2iPA1, and 3.2iPA2. Recording protocol is shown on the top of panel C. Current density–voltage (I/V) curves from different constructs (C6) and quantitative analysis of averaged peak LVA I_{Ca} density (C7), $^*P < 0.05$, $^{**}P < 0.01$, and $^{***}P < 0.001$, one-way ANOVA and Tukey post hoc test. (C8, C9) AAV-mediated 3.2iPA1 expression in PSNs significantly decrease $[Ca^{2+}]_c$. Depolarization for 0.3 seconds by 50 mM K^+ increased $[Ca^{2+}]_c$, which was blocked by TTA-P2 in the PSNs of naïve rats, and this effect was precluded by AAV-mediated 3.2iPA1 expression in PSNs; $^{***}P < 0.001$, one-way ANOVA and Tukey post hoc test. (D) No effects of 3.2iPAs on HVA I_{Ca} in DRG neurons. Typical HVA I_{Ca} traces in a small-sized neuron from a naïve rat show a threshold for activation approximately −30 mV and a maximum current amplitude activation at −10 mV, displaying small inactivation. Typical traces of HVA I_{Ca} recorded at −10 mV of neurons (<35 μm in diameter) from a sham-operated rat and naïve rats injected with AAV6-encoding GFP, 3.2NP, 3.2iPA1, and 3.2iPA2 (D1-D6). (D7) HVA I_{Ca} density–voltage (I/V) curves and (D8) quantitative analysis of averaged peak HVA I_{Ca} density, $P > 0.05$, one-way ANOVA and Tukey post hoc test. AAV, adeno-associated virus; ANOVA, analysis of variance; $Ca_V3.2$, calcium channels 3.2; DRG, dorsal root ganglia; I_{Ca}, calcium channel current; iPA, inhibitory peptide aptamer; HVA I_{Ca}, high-voltage–activated calcium current; $I_{Na1.7}$, $Na_V1.7$ current; I_K, potassium current; LVA I_{Ca}, low-voltage–activated calcium current; $Na_V1.7$, sodium channel 1.7; PSN, primary sensory neuron.

3.5. Inhibition of LVA but not high-voltage–activated calcium channels by 3.2iPA1 and 3.2iPA2 in rat primary sensory neurons

Because no heterologous system or cell lines can fully mimic in vivo conditions of sensory neurons, we further tested the functional inhibition of calcium channels by $Ca_V3.2$iPAs (3.2iPAs) in DRG PSNs. AAV6 vectors encoding 3.2NP, 3.2iPA1, 3.2iPA2, and 3.2iPA3 (all fused with GFP) were injected into L4/5 DRG of naïve rats (male), and acutely dissociated sensory neurons from DRG were tested at 4 weeks postinjection. Whole-cell voltage-clamp recordings from small-sized/medium-sized PSNs showed that AAV-mediated expressions of 3.2iPA1 and 3.2iPA2 produced significant inhibition of peak LVA I_{Ca} (pA/pF) by approximately 70% and 60%, respectively, whereas 3.2iPA3 enhanced peak LVA I_{Ca} by approximately 30%, compared with control PSNs. No change of peak LVA I_{Ca} was observed in PSNs expressing 3.2NP compared with that in naive cells (**Fig. 4C**). To further test the effects of 3.2iPA1 on Ca^{2+} influx through PSN $Ca_V3.2$/T-type channels, Ca^{2+} microfluorimetry was performed. Dissociated PSNs were depolarized by exposure to 50 mM K^+ for 0.3 seconds to selectively activate T-type channels[59] and in the presence of tetrodotoxin (TTX, 1 μM) to eliminate action potential generation, as previously described.[59] Results showed that AAV-mediated 3.2iPA1 expression in PSNs significantly depressed Ca^{2+} influx under these conditions. Patch-clamp recordings

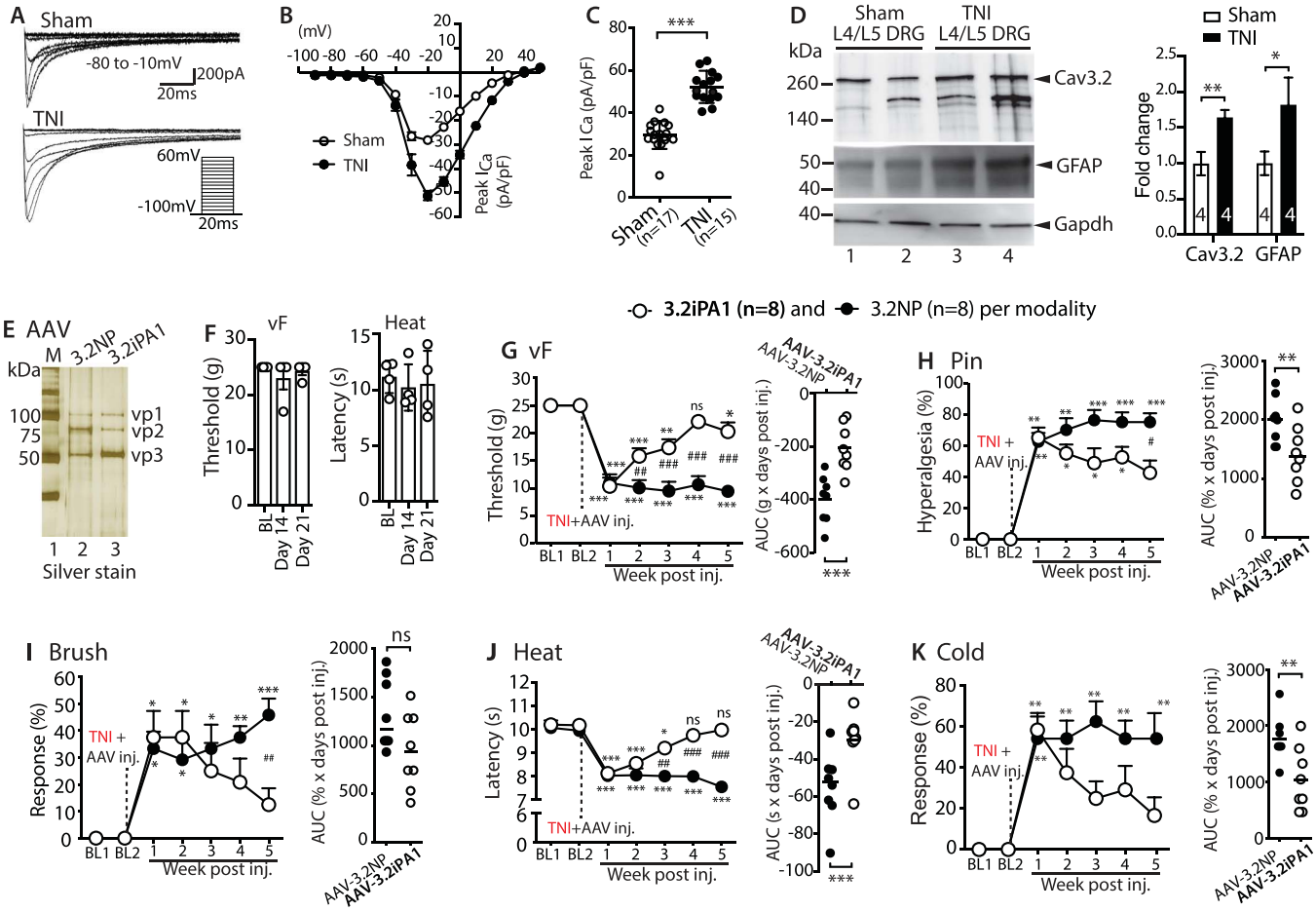

Figure 5. Prevention of tibial nerve injury–induced hypersensitivity by AAV6-3.2iPA1 (male rats). Representative traces of T-type $I_{Ca,}$ I/V curves and peak I_{Ca} densities from L4/L5 PSNs dissociated from sham and TNI rats 4 weeks after injury (A–C); $P < 0.001$, two-tailed Student *t* tests. Representative immunoblots of Cav3.2, GFAP, and GAPDH (D) with bar charts (right panel) showing densitometry analysis, $^{*}P < 0.05$ and $^{**}P < 0.01$ by two-tailed unpaired Student *t* test. Silver stain of purified AAV6-3.2NP and AAV6-3.2iPA1 (E). No difference of the sensitivity to vF and to heat at baseline, day 14, and day 21 after AAV6-3.2iPA1 injection (L4/L5 DRG) in sham rats (n = 4) (F). The time courses for the group averages of sensitivity to vF (G), hyperalgesia after touch with a pin (H), dynamic brush (I), sensitivity to heat (J), and acetone stimulation (K), before TNI and after TNI and immediately followed by DRG injection of either AAV6-3.2NP (n = 8 rats) or AAV6-3.2iPA1 (n = 8 rats). $^{*}P < 0.05$, $^{**}P < 0.01$, and $^{***}P < 0.001$ for comparison with BL within group and $\#P < 0.05$, $\#\#P < 0.01$, and $\#\#\#P < 0.001$ for comparison between groups after treatment, respectively (G and J), repeated measures two-way ANOVA and Turkey or Bonferroni post hoc test; (H, I, and K) nonparametric analyses by Friedman and Dunn post hoc test. Right panels of G–K show averaged AUC calculated for each individual for the period after vector injection. $^{**}P < 0.01$ and $^{***}P < 0.001$ for AUC comparison between groups (unpaired two-tailed Student *t* tests for vF and heat; the Mann-Whitney *U* tests for pin, brush, and cold). AAV, adeno-associated virus; ANOVA, analysis of variance; AUC, area under the curve; Ca_V, calcium channels 3.2; DRG, dorsal root ganglia; I_{Ca}, calcium channel current; ns, no significance; PSN, primary sensory neuron; TNI, tibial nerve injury; vF, von Frey test.

showed no effect of 3.2iPA1 and 3.2iPA2 on peak HVA I_{Ca} (**Fig. 4D**). Of importance, AAV-encoded 3.2iPA1 expression in vivo did not affect BL mechanical (vF) and thermal (heat) thresholds in control rats (see further). Because these findings support that 3.2iPA expression in PSNs is a means of selectively inhibiting LVA I_{Ca}, further testing was performed in vivo to evaluate their analgesic potential.

3.6. Attenuation of tibial nerve injury–induced hypersensitivity by AAV6-3.2iPA1 in vivo (male rats)

3.6.1. Pilot testing of 3.2iPA1

To detect $Ca_V3.2$ protein expression, we first examined the specificity of $Ca_V3.2$ antibody by immunoblotting on cell lysates of stable cell lines expressing different calcium channels, which showed detection of $Ca_V3.2$ but not $Ca_V3.1$, $Ca_V3.3$, or $Ca_V2.2$ (Suppl. Fig. 2A, available at http://links.lww.com/PAIN/B621). Immunoblots using this antibody on DRG samples from naïve rats revealed that $Ca_V3.2$ protein was more abundant in the cytosolic and nuclear fractions than in the PM under our preparation conditions (Suppl. Fig. 2B, available at http://links.lww.com/PAIN/B621). Immunohistochemistry using this antibody revealed Cav3.2 detection preferentially in small-sized and medium-sized PSNs (Suppl. Fig. 2C and D, available at http://links.lww.com/PAIN/B621). These results confirmed the specificity of the Cav3.2 antibody used in this study to detect Cav3.2 expression by IHC and immunoblots.

Pilot in vivo tests were initiated to evaluate whether AAV-mediated $Ca_V3.2$iPA1 expression selectively in the PSNs could reduce development of pain behaviors after nerve injury. We first observed that TNI enhanced PSN Cav3.2/T-type channel activity and increased Cav3.2 and GFAP expressions (**Figs. 5A–D**), as in previous reports.[16] To test potential analgesia, AAVs expressing GFP-fused 3.2iPA1, or 3.2NP as a control, were packaged into serotype 6 (**Fig. 5E**) because this serotype efficiently transduces nociceptive PSNs, which express $Ca_V3.2$.[40,90] Evoked pain behaviors were tested by sensory

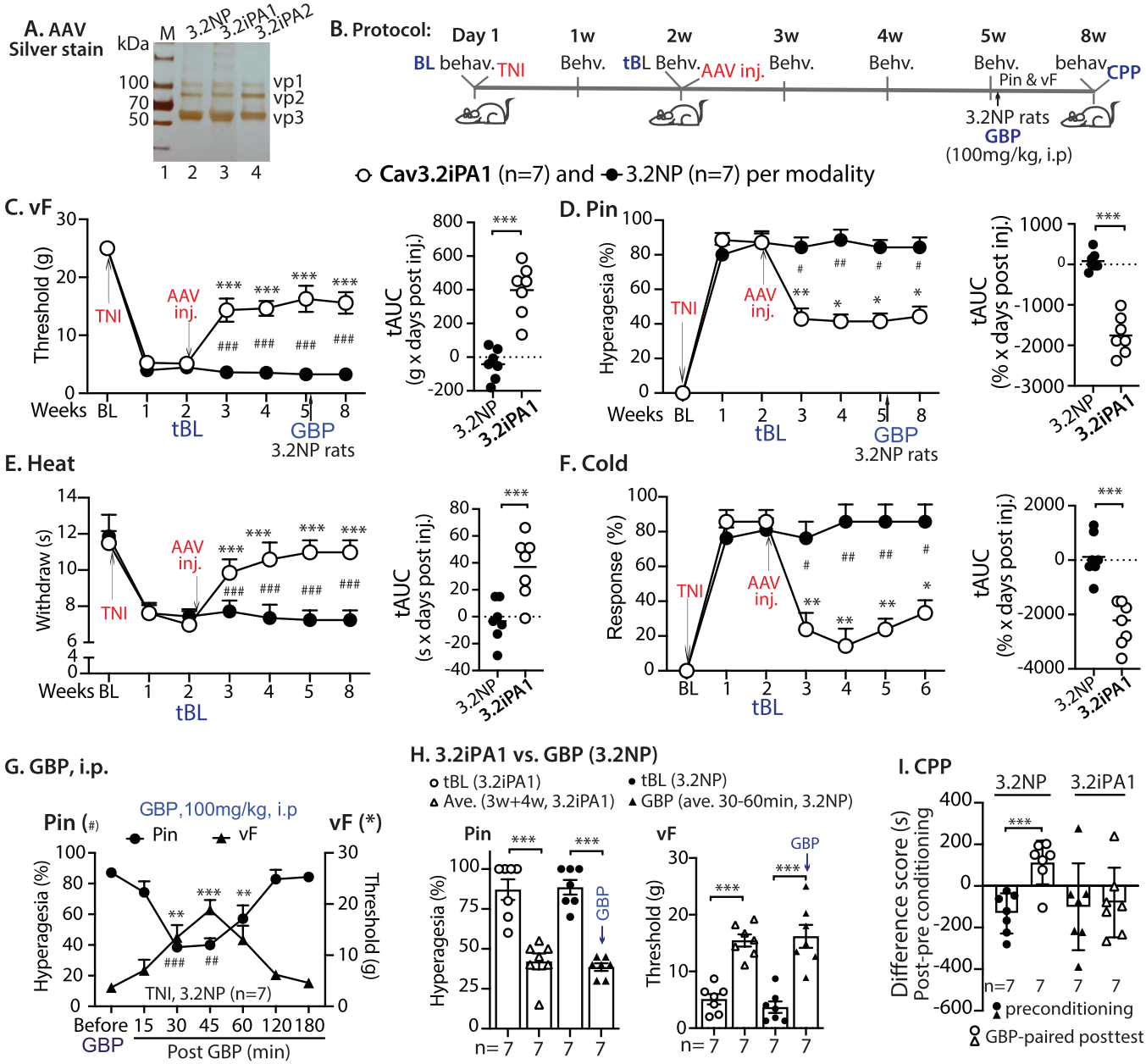

Figure 6. Treatment of established neuropathic pain by dorsal root ganglia AAV6-3.2iPA1 (male rats). New lots of purified AAVs (A, silver stain) were prepared for the experiment in an animal protocol schematically outlined (B). AAV6-3.2iPA1 treatment: The time courses for the group averages of sensitivity to vF, pin, heat, and cold before and after DRG injection of either AAV6-3.2iPA1 (n = 7) or AAV6-3.2NP (control, n = 7) (C–F) as indicated; $^{*}P < 0.05$, $^{**}P < 0.0,1$ and $^{***}P < 0.001$ for comparisons with the tBL within group and $\#P < 0.05$, $\#\#P < 0.01$, and $\#\#\#P < 0.001$ for comparisons between groups. Repeated measures parametric two-way ANOVA for vF and heat, followed by the Tukey (within group) and Bonferroni (between group) post hoc tests; and nonparametric Friedman ANOVA for Pin and cold tests and Dunn post hoc test. Right panels of C-F show tAUC calculated using measures 14-day post TNI and before vector injection as tBL; $^{***}P < 0.001$, comparisons of tAUC between groups (unpaired, two-tailed Student *t* tests for vF and heat, and Mann-Whitney *U* tests for pin and cold). (G) the time courses (3 hours) of sensitivity to vF and pin injected with GBP (100 mg/kg, i.p.) in TNI+AAV-3.2 PN rats, performed at the time point as indicated in (B–D); $^{**}P < 0.01$ and $^{***}P < 0.001$ vs before GBP, repeated measures two-way ANOVA for vF with Tukey post hoc test, and $\#\#P < 0.01$, and $\#\#\#P < 0.001$ for Pin Friedman analysis and Dunn post hoc test. (H) Comparison of the efficacy between AAV-3.2iPA1 treatment in TNI and GBP (i.p.) anticonception in 3.2NP rats by vF and Pin tests, $^{***}P < 0.001$, unpaired two-tailed Student *t* test for vF and Mann-Whitney *U* test for Pin. Pin (%, TNI + 3.2iPA1): tBL 87 ± 6 and after treatment 42 ± 4, Pin (%, TNI + 3.2NP): before injection 88 ± 5 and after GBP 39 ± 2. vF (g, TNI + 3.2iPA1): tBL 5 ± 1 and after treatment 15 ± 1, vF (g, TNI + 3.2NP + GBP): before injection 4 ± 1 and after GBP 16 ± 2 ($P > 0.05$, unpaired two-tailed Student *t* test for vF and Mann-Whitney *U* test for Pin). (I) the results of the CPP difference scores (seconds, s) of preconditioning chamber and of the GBP-paired chamber between AAV-3.2iPA1 (n = 7) and AAV-3.2NP (control, n = 7), $^{***}P < 0.001$ (unpaired, two-tailed Student *t* test). AAV, adeno-associated virus; ANOVA, analysis of variance; BL, baseline; DRG, dorsal root ganglia; GBP, Gabapentin; CPP, conditioned place preference; i.p, intraperitoneal; TNI, tibial nerve injury; tBL, treatment baseline; tAUC, treatment area under curve.

stimuli applied to the lateral margin of the plantar aspect of the paw in the sural area of innervation, as previously described.[78,93] Initial experiments showed that AAV-3.2iPA1 treatment did not affect mechanical (vF) or thermal (heat) thresholds in control rats (nerve exposure without ligation, **Fig. 5F**). To test analgesic effects in the context of neuropathic pain, this pilot experimental design involved performing the TNI operation and DRG-AAV injections at the same operation in adult rats (**Figs. 5G–K**). Rats were randomized to receive intraganglionic vector injection of either AAV6-3.2iPA1 or AAV6-

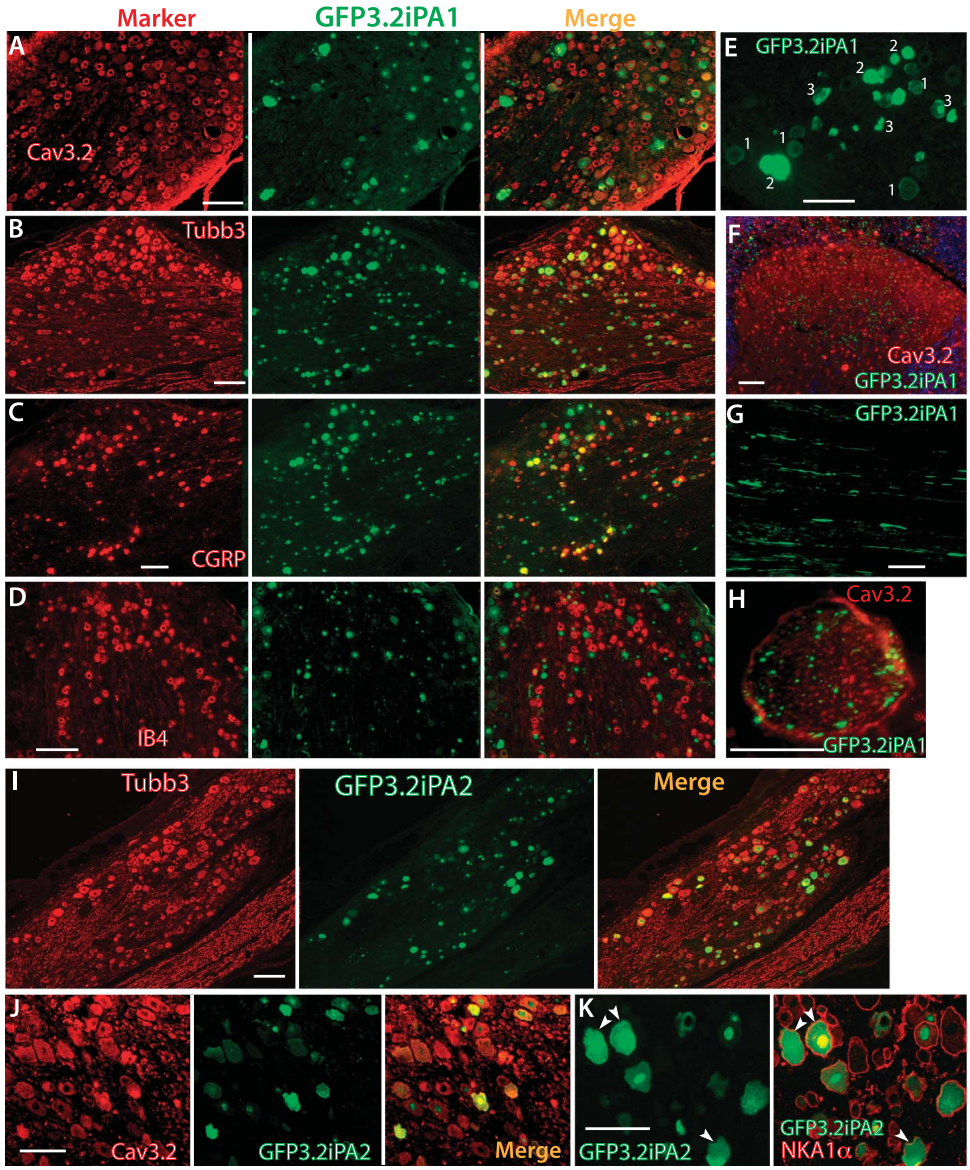

Figure 7. Immunohistochemistry characterization of 3.2iPAs expression in vivo (male). Illustration shows representative IHC images of 3.2iPA1 (A–H) and 3.2iPA2 (I-K) on the sections from L4/L5-DRG of TNI rats 6 weeks after treatment. IHC montage images show GFP-3.2iPA1 expression (green), colabeled with $Ca_V3.2$ (A, red), Tubb3 (B, red), CGRP (C, red), and IB4 (D, red). An IHC image shows multiple PSN cellular localization of GFP-3.2iPA1; 1, 2, and 3 denote the patterns of localization in PM, cytosol fractions, and nuclear fractions, respectively (E). (F–H) IHC images show GFP-$Ca_V3.2$iPA1 expression (green) colabeled with $Ca_V3.2$ (red) in the neuropil of ipsilateral spinal DH (F, dashed lines outline DH), sciatic nerve (G), and in afferent terminals colabeled with $Ca_V3.2$ (red) (H) within the dermis of ipsilateral hindpaw. (I) IHC montage images of GFP-$Ca_V3.2$iPA2 expression (green), colabeled with Tubb3 (red), showing colocalization in merged image. (J) IHC montage images of GFP-$Ca_V3.2$iPA2 expression (green), colabeled with Cav3.2 (red), showing colocalization in the merged image. GFP-3.2iPA2 displays multiple cellular localization in PSNs, including cytosol fractions, nuclear fractions, and PM. Arrowheads point to NKA1α (red) and GFP-3.2iPA2 (green) colabeled PM (K, merged image). Scale bar: 50 μm for all images. $Ca_V3.2$, calcium channels 3.2; CGRP, calcitonin gene–related peptide; DRG, dorsal root ganglia; GFAP, glial fibrillary acidic protein; IB4, Isolectin IB4; IHC, immunohistochemistry; iPA, inhibitory peptide aptamer; NKA1a, sodium/potassium ATPase 1α; PM, plasma membrane; PSN, primary sensory neurons; Tubb3, b3-tubulin; TNI, tibial nerve injury.

3.2NP into both the ipsilateral L4 and L5 DRG immediately after TNI surgery. Rats given the control vector (AAV6-3.2NP) developed significant pain behaviors after TNI, which included lowered withdrawal threshold from mild mechanical stimuli (vF and brush testing), more frequent hyperalgesic-type responses (sustained lifting, shaking, and grooming) after noxious mechanical stimulation (Pin testing), reduced withdrawal threshold to heat, and more frequent withdrawals from cold (acetone stimulation), which persisted after injection during the 5 weeks of the observation course. By contrast, rats injected with AAV6-3.2iPA1 showed initial development of similar hypersensitivity at 1 week, but this was followed by a gradual reversal of these changes. These findings suggest that DRG-targeted $Ca_V3.2$-iPA1 treatment has analgesic efficacy in reducing peripheral hypersensitivity in TNI rats.

3.6.2. Treatment of established neuropathic pain by dorsal root ganglia-AAV6-3.2iPAs

Having ascertained the potential for in vivo analgesia, we extended our experiments to evaluate the effectiveness of DRG-AAV6-3.2iPAs (iPA1 and iPA2) in a more clinically relevant

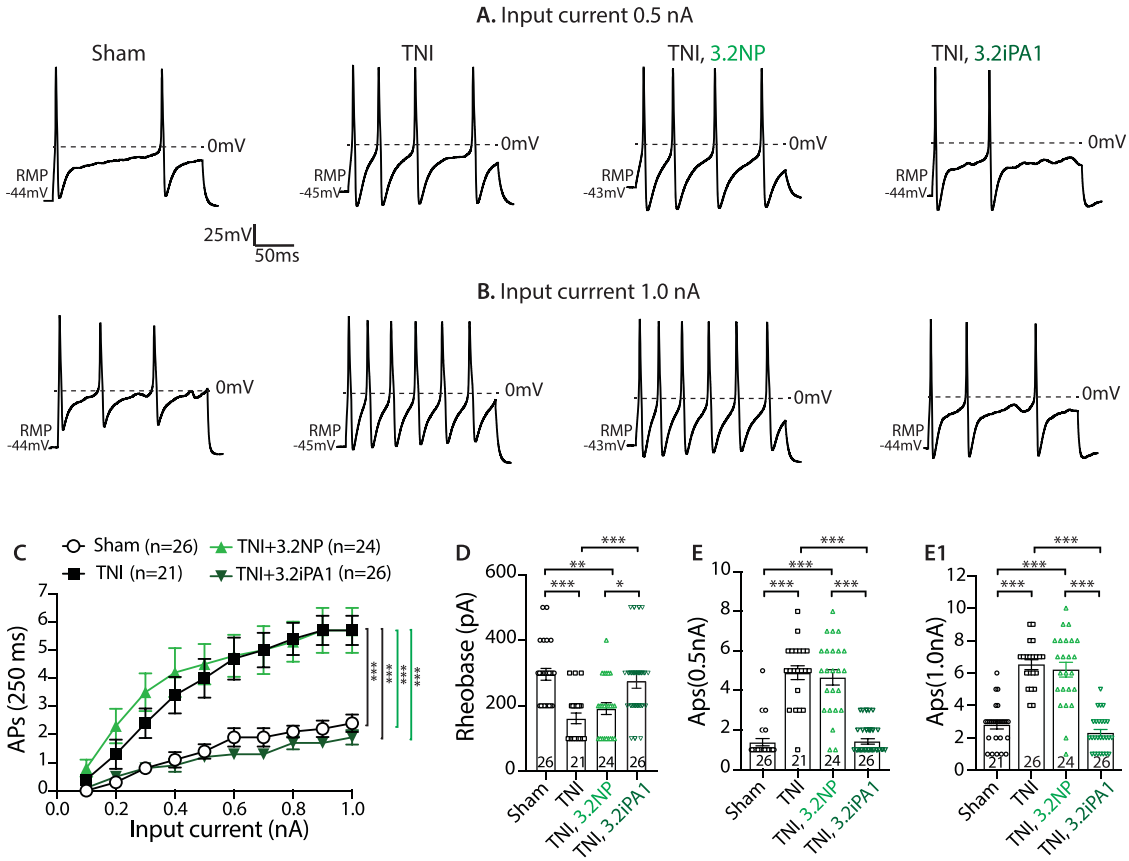

Figure 8. Current-clamp analysis of AAV6-3.2iPA1 transduction on dorsal root ganglia neuronal excitability (male). Representative AP traces elicited by 250 ms depolarizing current of 0.5 nA (A) and 1.0 nA (B) (same cells) from RMP were recorded from DRG neurons dissociated from the rats of sham, TNI, and GFP-expressing neurons in TNI treated with AAV6-3.2NP or AAV6-3.2iPA1, as indicated. Comparison of responses (number of APs evoked by a 250 ms stimulus) for the populations of DRG neurons in different groups across a range of step current injections from 0.1 to 1.0 nA (C); ***$P < 0.001$, two-way ANOVA of main effects of groups with Bonferroni post hoc test. Scatter plots with bars show analysis of the rheobases (D) and AP numbers evoked by input current at 0.5 nA (E) and 1.0 nA (E1) from RMP, respectively. The number in each group is the number of analyzed neurons per group. *, **, and ***denote $P < 0.05$, 0.01, and 0.001, respectively. One-way ANOVA and Turkey post hoc tests. RMP, rest membrane potential; AAV, adeno-associated virus; ANOVA, analysis of variance; AP, action potential; DRG, dorsal root ganglia; RMP, resting membrane potential; TNI, tibial nerve injury.

design involving reversal of established pain behavior, including both evoked responses as well as spontaneous ongoing pain after TNI (**Fig. 6A**). New preparations of vectors of AAV6-3.2iPA1, AAV6-3.2iPA2, or AAV6-3.2NP (control), consisting of iPAs or NP fused with GFP, were generated for these experiments. In the experimental design, the sensitivity to mechanical and thermal cutaneous stimulation was assessed at baseline and weekly after TNI for 2 weeks before AAV injection. Thereafter, rats were randomized to receive intraganglionic injection of either AAV6-3.2iPA1, AAV6-3.2iPA2, or AAV6-3.2NP into the ipsilateral L4/L5 DRG, after which sensory behavior was evaluated weekly for 6 weeks. A single-dose GBP (100 mg/kg, i.p.) was injected in animals that had received AAV6-3.2NP 3 weeks previously, as a positive control. The GBP-CCP test was performed in all groups as a terminal experiment to evaluate spontaneous pain. Behaviors measured before vector injection at the 14th day after TNI were used as a treatment BL (tBL) to evaluate effectiveness of vector treatments (**Fig. 6B**). Tissues were harvested for IHC characterization of transgene and target gene expression and for whole-cell current-clamp AP recording of neuronal excitability on dissociated DRG neurons.

All rats established multiple modalities of pain behavior 2 weeks after TNI, including lowered threshold for withdrawal from mild mechanical stimuli (vF testing), more frequent hyperalgesic-type responses after noxious mechanical stimulation (Pin testing), and hypersensitivity to heat and acetone stimulation. These behaviors persisted after injection of the control AAV6-3.2NP during the 6 weeks of observation course. By contrast, rats injected with AAV6-3.2iPA1 showed reversal of these changes, which persisted throughout the observation period (**Figs. 6C–F**). GBP applied between the third and fourth weeks in TNI+ AAV6-3.2NP rats reversed mechanical hypersensitivity at 30 to 60 minutes after GBP, but animals were fully mechanically hypersensitive again 3 hours after injection (**Fig. 6G**). For animals treated with AAV-3.2iPA1, the averaged (3w+4w) allodynia (vF) and hyperalgesia (Pin) showed approximately 60% reversal to tBL, which was comparable with the averaged (30-60 minutes) response to GBP in AAV6-3.2NP group (**Fig. 6H**). Using a biased CPP paradigm,[60] the effect of AAV-3.2iPA1 treatment on spontaneous pain was evaluated. None of the animals in either group were excluded from study because of their BL preference/avoidance for a chamber.[60] A significant CPP effect of GBP administration was observed in the TNI rats injected with AAV6-3.2NP, whereas there was no significant difference in the time spent in the initially nonpreferred chamber during BL vs testing period in AAV-3.2iPA1–treated TNI animals, indicating AAV-3.2iPA1 treatment relieved ongoing spontaneous pain in TNI rats (**Fig. 6I**). A comparable analgesic effectiveness for both evoked and spontaneous pain behaviors was observed for AAV-3.2iPA2 treatment in the established pain induced by TNI (Suppl. Fig. 3, available at http://links.lww.com/PAIN/B621), as described earlier for AAV-3.2iPA1. This could be expected on the basis

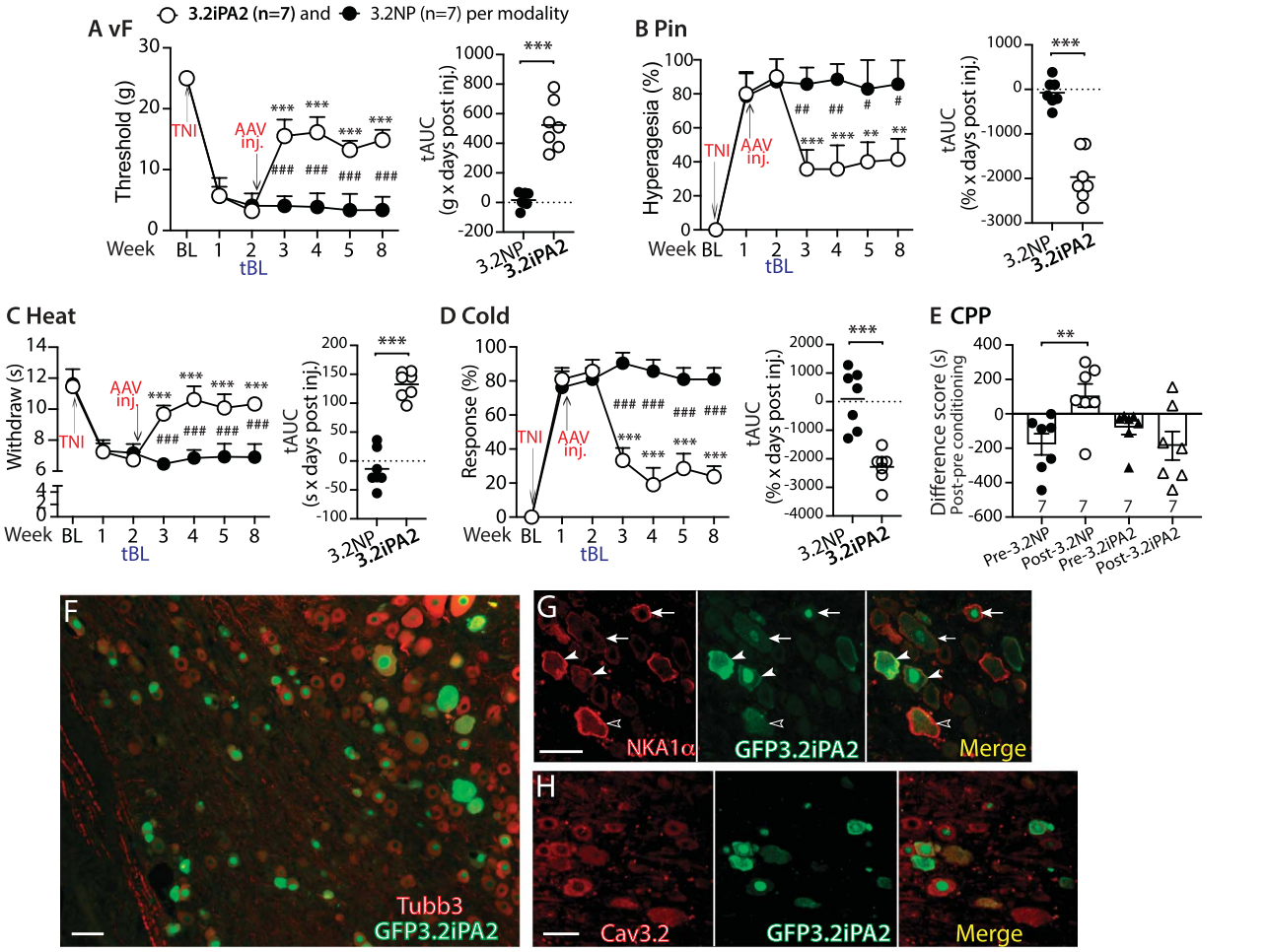

Figure 9. Analgesia of dorsal root ganglia-AAV6-3.2iPA2 treatment in female tibial nerve injury rats. Analogous figures to Fig. 6 and suppl. Fig. 3 (available at http://links.lww.com/PAIN/B621) show significant analgesia after DRG delivery of AAV6-3.2iPA2 in established TNI pain behavior in female rats. $^{**}P < 0.0.1$ and $^{***}P < 0.001$ for comparisons to the treatment baseline (tBL) within group and $\#P < 0.05$, $\#\#P < 0.01$, and $\#\#\#P < 0.001$ for comparisons between groups (A–D). Repeated measures parametric two-way ANOVA for vF and Heat, followed by Tukey (within group) and Bonferroni (between group) post hoc tests; and nonparametric Friedman ANOVA for Pin and Cold tests and Dunn post hoc. Right panels of A to D show tAUC calculated using measures 14-day post-TNI and before vector injection as tBL; $^{***}P < 0.001$, comparisons of tAUC between groups (unpaired, two-tailed Student *t* tests for vF and Heat, and Mann-Whitney *U* tests for Pin and cold). Conditioned place preference difference scores (s) of preconditioning chamber and of the GBP-paired chamber between AAV-3.2iPA2 (n = 7) and AAV-3.2NP (control, n = 7), $^{**}P < 0.01$ (unpaired, two-tailed Student *t* test) (E). Representative IHC overlaid images (GFP3.2iPA2 with Tubb3) show neuronal expression profile 6 weeks after AAV-3.2iPA2 injection (F), multiple cellular localization (G, arrows and arrowheads point to nuclear and PM, respectively), colocalization of GFP-3.2iPA2 with Cav3.2 (H). Scale bar: 50 μm for all images. AAV, adeno-associated virus; ANOVA, analysis of variance; BL, baseline; $Ca_V3.2$, calcium channels 3.2; DRG, dorsal root ganglia; IHC, immunohistochemistry; PSN, primary sensory neuron; tBL, treatment baseline; tAUC, treatment area under the curve; TNI, tibial nerve injury.

that both 3.2iPA1 and 3.2iPA2 displayed similar inhibitory effects on $I_{Ca3.2}$ without changing Cav3.2 biophysical features (**Fig. 2**).

A histological examination (**Fig. 7**) determined the in vivo transduction rate for AAV6-3.2iPA1 6 weeks after vector injection. The 3.2iPA1-positive neurons (GFP) comprised 48 ± 5% (971 of 1898 total neuronal profiles) identified by pan-neuronal marker β3-tubulin (n = 3 DRG, 5 sections per DRG, selected as every fifth section from the consecutive serial sections). Transduced DRG neurons included the full-size range of the PSNs that also expressed $Ca_V3.2$, and 3.2iPA1 expression showed multiple subcellular localizations, including PSN cytosol, nucleus, and plasma membrane, but not in perineuronal glia cells. The 3.2iPA1-IR signals (GFP) were additionally detected in spinal dorsal horn neuropil, sciatic nerve, and hindpaw afferent terminals. In vivo transduction profile of AAV6-3.2iPA2 showed multiple PSN subcellular expressions (**Figs. 7I–K**), similar to AAV6-3.2iPA1.

Cumulatively, these findings suggest that treatment with AAV6-mediated expression of Cav3.2iPA1 and 2 targeted to sensory neurons in the DRG has clear analgesic effectiveness in normalizing the established peripheral hypersensitivity for both evoked and spontaneous pain in a rat neuropathy model in a sustained fashion.

3.7. Reversal of primary sensory neuron hyperexcitability by AAV6-3.2iPA1 treatment (male rats)

Cav3.2 channels contribute to nociception by lowering the threshold for excitability in PSNs.[26] We therefore determined whether AAV6-3.2iPA1 treatment reverses the enhanced neuronal excitability of nociceptive PSNs after TNI,[78] using the whole-cell current-clamp AP recording of DRG dissociated neurons from rats after the treatment protocol shown in **Figure 6B**. Although TNI results in DRG with comingled injured and uninjured axons, nerve injury can induce an increase of voltage-gated ion channel activity in both axotomized neurons and adjacent intact neurons, leading to similar electrophysiological changes and increased discharge frequency in axotomized and neighboring

intact DRG neurons.[13] We therefore recorded from randomly chosen small-sized and medium-sized neurons (<40 μm in diameter)[77] in the cultures from dissociated L4 and L5 DRGs. Transduced neurons were identified using GFP fluorescence, and excitability was evaluated by measuring rheobase and repetitive firing during 250-ms current injection steps. Results showed that the averaged rheobase in the neurons from TNI rats was significantly decreased, and the frequency of APs evoked in neurons from TNI rats was significantly increased, compared with sham controls. These were normalized in transduced neurons after AAV6-3.2iPA1 treatment, whereas 3.2NP-transduced neurons had no significant effect (**Fig. 8**). We did not test the effects of 3.2iPA2 on TNI-induced PSN hyperexcitability. However, reversal of TNI-induced PSN hyperexcitability by AAV6-3.2iPA2 treatment is expected, as has been reported that inhibition of $Ca_V3.2$ channels by a homologous peptide to iPA2 reverses hyperexcitability of peripheral nociceptors and alleviates postsurgical pain.[40] These findings indicate that reversal of nerve injury–induced sensory neuron hyperexcitability by Cav3.2iPAs may contribute to its attenuation of neuropathic pain behaviors.

3.8. Analgesia of dorsal root ganglia-AAV6-3.2iPA2 treatment in female tibial nerve injury rats

Sex differences exist in experimental and clinical pain and in responsivity to interventions.[53] We therefore next test whether DRG-AAV6-3.2iPA treatment is also effective in attenuating hypersensitivity induced by TNI in female animals. A treatment protocol similar to the tests in male animals (**Fig. 6**) was conducted. Specifically, vector injection was performed 2 weeks after TNI, and both evoked mechanical and thermal nociception, as well as GBP-CPP were evaluated. The same batch preparation of AAV6-3.2iPA2 tested in male rats was used for testing (AAV6-3.2iPA1 was not applied because these 2 treatment vectors showed comparable antinociceptive effects in male TNI rats, described in **Fig. 6** and Suppl. Fig. 3). Results showed that the female rats displayed similar phenotypic development of hypersensitivity after induction of TNI to male rats and both evoked mechanical/thermal hypersensitivity and GBP-CPP responses were normalized after AAV6-3.2iPA2 treatment, demonstrating a comparable analgesic effect to the male animals (**Figs. 9A–E**). Immunohistochemistry on the DRG sections from female TNI rats 6 weeks after AAV6-3.2iPA2 injection also revealed GFP-3.2iPA2 expression profile comparable with that of male rats (**Figs. 9F–H**). Thus, although not rigorously compared, a sexual dimorphism seems not apparent for both pain behavior phenotypes after TNI and in responsivity to DRG-3.2iPA2 treatment in our studies.

4. Discussion

The ongoing opioid crisis in the United States has spurred efforts to develop nonopioid drugs for treating chronic pain, but these efforts have mostly failed.[84] New therapeutic approaches are therefore needed. The $Ca_V3.2$/T-type channels are key elements regulating sensory neuron excitability and shaping multiple modalities of sensory perception and pain signal amplification, and the roles of $Ca_V3.2$ channels of the peripheral sensory pathways in pain sensation are well established.[10] Thus, $Ca_V3.2$ channels are an important class of targets for drugs that are needed for the clinical treatment of chronic pain.[63,85] Not only do $Ca_V3.2$ channelopathies underlie a critical mechanism for a variety of pain conditions, but modifying $Ca_V3.2$ function has proved to be a useful preclinical intervention in the treatment of chronic pain.[48] In addition, both $Ca_V3.1$ and $Ca_V3.3$ are also confirmed pain mediators.[55,56] These observations underlie our motivation for the experiments reported here.

In this study, we used a combined in silico and experimental strategy to design iPAs by targeting $Ca_V3.2$ IDRs. Promising $Ca_V3.2$iPA candidates were selected and validated using in vitro cell line-based and ex vivo PSN-based methods. Expression of these $Ca_V3.2$iPAs inhibits T-type/Cav3.2 and Cav3.1 currents but not Cav3.3 calcium currents. Because the steady-state properties of $Ca_V3.2$ channels are not affected, it is therefore possible that iPAs may reduce $Ca_V3.2$/Cav3.1 T-type channel conductance possibly by a direct or indirect channel occupancy or by decreased channel numbers in the membrane due to altered trafficking or transcription/translation. Of importance, AAV-mediated expression of the prototypes $Ca_V3.2$iPA1 and $Ca_V3.2$-iPA2 restricted to DRG neurons produces sustained inhibition of I_{Ca} conducted by $Ca_V3.2$/Cav3.1 T-type channels in PSNs and attenuates established nerve injury–induced pain behavior in both male and female rats, effective for both evoked mechanical and thermal hypersensitivity and ongoing or spontaneous pain behavior, which are symptoms commonly found in patients experiencing multiple types of painful neuropathy.[42] Overall, our results indicate that targeting IDRs facilitates identification of druggable T-type iPAs and $Ca_V3.2$iPAs are promising analgesic leads with potentials for translational clinical analgesia.

Research efforts have helped us better understanding the pathobiological role of $Ca_V3.2$ in chronic pain. Progress has been made over the past decade to develop more selective and efficacious T-type/$Ca_V3.2$ blockers to treat pain.[47,89] However, the clinically available small molecule $Ca_V3.2$ blockers used to treat pain applied systemically and orally are nonselective across different tissues and contribute to off-site effects because $Ca_V3.2$ are widely expressed throughout the body of mammals involving in a wide variety of physiological functions. Thus, despite preclinical studies demonstrating that decreased T-type/$Ca_V3.2$ activity induces a reduction in pain, few molecules targeting this gene product have reached the final phase of clinical trials,[6,42,43,47,81,98] and many small molecules targeting T-type/$Ca_V3.2$ have failed to be validated as pain therapy drugs.[1,79] Thus, development of novel peripheral acting strategies for T-type/$Ca_V3.2$ inhibition would be an ideal approach for clinical pain treatment.

Chronic pain in almost all cases is maintained by ongoing afferent hyperactivity originating from peripheral pathological sources.[5,69] Primary sensory neurons not only initiate nociception but also play a central role in the development and maintenance of painful neuropathies.[13] Pain-sensing DRG-PSNs can become hyperexcitable in response to pathological conditions such as peripheral nerve injury, which in turn leads to the development of neuropathic pain. Multiple lines of evidence from both preclinical and clinical studies demonstrate that block of peripheral nociceptive input can effectively relieve pain symptoms, including spontaneous pain.[23,31] Therefore, treatments targeting the peripheral neurons both avoid CNS side effects and are likely to succeed. Indeed, a recent expert commentary states, “activity in primary afferent neurons represents a ‘low-hanging target’ in the development of safe therapies” for patients with chronic pain.[69] Delivering drugs to the peripheral nervous system is well developed and safe, for instance, as used in clinical anesthesia for regional blockade and by pain physicians for diagnosis and treatment of radiculopathy.[65] Injection into the DRG has minimal consequences in preclinical models.[24] It has also been demonstrated that unintentional intraganglionic injection commonly accompanies clinical foraminal epidural steroid injection,[65] a very common procedure with minimal risk of nerve damage. Thus, the

PSNs are particularly suitable for targeting new analgesic treatments, especially at the level of the associated pathological DRG.[8,33,38,60]

Our approach used here includes a novel strategy in which highly selective and nontoxic $Ca_V3.2$iPAs are designed and developed from $Ca_V3.2$ IDRs, and these are delivered by using AAV in an anatomically targeted fashion that restricts block of T-type $Ca_V3.2$/Cav3.1 to the peripheral nerves. In preclinical models, direct DRG delivery of AAVs encoding analgesic biologics can provide relief in chronic pain, with high transduction efficiency, flexibility for selective segmental localization, and minimal behavioral changes attributable to the surgical procedure.[9,51,93] In parallel, injection techniques are being advanced to achieve minimally invasive delivery of biologics for future clinical pain therapy.[66–68] Small peptides that mimic target protein sequences can serve as decoy molecules to selectively interfere with the function of their target signaling protein by preemptively binding to it.[25,93] We have successfully used this strategy in rat models to induce analgesia by preventing assembly of functional transient receptor potential cation channel subfamily V member 1 (TrpV1) channels[87] and by blocking membrane trafficking of $Ca_V2.2$ channels by interrupting their interactions with the structural protein collapsin response mediator protein 2 (CRMP2).[25,93] Here, we extend the applicability of DRG-AAV strategy to the analgesic effectiveness of PSN T-type/$Ca_V3.2$ blockade for neuropathic pain. The multipronged feature of Cav3.2iPA1/2 with combined $Ca_V3.2$ and Cav3.1 inhibition restricted in PSNs might be an additional analgesic advantage because both are known nociceptive hubs.[40,56] We believe that our promising results showing effectiveness and tolerability, if proving long-term efficacy and absence of adverse events, suggest the utility of the approach for developing therapeutic reagents. Because activation of T-type/$Ca_V3.2$ has been found in various pain conditions, it will be of interest to address the analgesic efficacy of AAV-$Ca_V3.2$iPAs for PSN T-type/$Ca_V3.2$ inhibition in additional models of other pain etiologies.

Injury-induced ectopic hyperactivity of PSNs causes hypersensitization in multiple sites of the peripheral sensory nervous system, including augmented pain perception in the peripheral terminals, enhanced nociceptive signal transduction in PSN soma and T-junction, and increased neurotransmission in the spinal dorsal horn.[18,26,39] At this early stage, our studies did not investigate differential actions by block of T-type/$Ca_V3.2$ along the pathway of nociceptors nor did the results rule out the possibility that block of T-type/$Ca_V3.2$ reduces pain by inhibiting afferent hyperexcitable input, thus indirectly modulating spinal cord and brain antinociceptive control circuits.[13,46,75] Although our studies have initially focused on testing whether targeting IDRs can facilitate discovery of T-type/$Ca_V3.2$ inhibitory peptides for AAV-mediated analgesia, how the identified $Ca_V3.2$iPA functioning remains unknown. The potential signaling pathways that the $Ca_V3.2$iPAs affected could be many because $Ca_V3.2$ intracellular segments serve as essential interfaces for many regulatory signaling molecules, including nuclear-localized deubiquitinating enzyme (USP5),[29] calcium/calmodulin–dependent protein kinase II,[35] cyclin-dependent kinase 5,[32] G-proteins,[64] calcineurin,[34] calmodulin,[15] syntaxin/SNAP25,[83] Kelch-like protein 1,[50] and Stac1.[74] In addition, $Ca_V3.2$ can form protein complexes with members of the K^+ channel family, such as K_V4, $K_{Ca3.1}$, and $K_{Ca1.1}$ (BK),[2,70] and K^+/Na^+ hyperpolarization–activated cyclic nucleotide-gated channel 1,[22] as well as lipids.[72] Alterations of these molecules and ionic channels after nerve injury are essential for ectopic PSN hyperactivity and pain.

In conclusion, our data describe a strategy that addresses a significant hurdle in $Ca_V3.2$ inhibitor discovered by targeting $Ca_V3.2$ IDRs. $Ca_V3.2$iPA1 and 2 are promising analgesic leads that, combined with AAV-targeted gene delivery in anatomically segmental sensory ganglia, have the potentials for future development as novel peripheral $Ca_V3.2$-targeting therapeutics in the treatment of intractable pain that cannot be controlled with current medical care. In addition, the IDR approach is also applicable of discovering iPAs to many other pronociceptive ion channels for AAV-mediated sensory neuron-specific analgesia. Finally, many questions are raised by this study, and the precise structural details and molecular mechanisms of $Ca_V3.2$iPAs for their $I_{Ca3.2}$ blockade remain to be identified. For example, what functional role may be served by $Ca_V3.2$iPAs in nuclei? Do $Ca_V3.2$iPAs regulate gene expression? Indeed, in searching for functional domains, high-score nuclear localization signals are identified in the sequences of $Ca_V3.2$iPAs and $Ca_V3.2$ protein (Suppl. Fig. 4, available at http://links.lww.com/PAIN/B621). To account this for an intriguing mechanism, it seems plausible that nuclear-localized $Ca_V3.2$iPAs may indirectly, at least partly, contribute to $I_{Ca3.2}$ inhibition by affecting calcium-regulated transcriptions of genes that are critical for $Ca_V3.2$ functions. Forthcoming studies will aim at addressing these questions.

Conflict of interest statement

The authors have no conflicts of interest to declare.

Acknowledgments

The authors thank Dr. Markus Missler (Westfalische Wilhelms University, Germany) for providing HEK293 Cav2.2 stable cell line and Dr. Bin Pan (MCW) for his technical assistance for voltage-gated patch-clamp recording experiments. This research was supported by a grant from a National Institutes of Health grant R61NS116203 (to H.Y. and Q.H.), an MCW NRC grant FP00016291 (to H.Y.), and 2022 award from Dr. Ralph and Marian Falk Medical Research Trust, Bank of America, Private Bank (to H.Y. and Q.H.).

Appendix A. Supplemental digital content

Supplemental digital content associated with this article can be found online at http://links.lww.com/PAIN/B621.

Supplemental video content

A video abstract associated with this article can be found at http://links.lww.com/PAIN/B622.

Article history:
Received 10 January 2022
Received in revised form 19 March 2022
Accepted 23 March 2022
Available online 14 April 2022

References

[1] Alles SRA, Smith PA. Etiology and pharmacology of neuropathic pain. Pharmacol Rev 2018;70:315–47.
[2] Anderson D, Mehaffey WH, Iftinca M, Rehak R, Engbers JD, Hameed S, Zamponi GW, Turner RW. Regulation of neuronal activity by Cav3-Kv4 channel signaling complexes. Nat Neurosci 2010;13:333–7.
[3] Bah A, Forman-Kay JD. Modulation of intrinsically disordered protein function by post-translational modifications. J Biol Chem 2016;291:6696–705.

[4] Barik A, Katuwawala A, Hanson J, Paliwal K, Zhou Y, Kurgan L. DEPICTER: intrinsic disorder and disorder function prediction server. J Mol Biol 2020;432:3379–87.
[5] Baron R. Mechanisms of disease: neuropathic pain—a clinical perspective. Nat Clin Pract Neurol 2006;2:95–106.
[6] Barton ME, Eberle EL, Shannon HE. The antihyperalgesic effects of the T-type calcium channel blockers ethosuximide, trimethadione, and mibefradil. Eur J Pharmacol 2005;521:79–85.
[7] Bernier LP, Blais D, Boue-Grabot E, Seguela P. A dual polybasic motif determines phosphoinositide binding and regulation in the P2X channel family. PLoS One 2012;7:e40595.
[8] Berta T, Qadri Y, Tan PH, Ji RR. Targeting dorsal root ganglia and primary sensory neurons for the treatment of chronic pain. Expert Opin Ther Targets 2017;21:695–703.
[9] Beutler AS, Reinhardt M. AAV for pain: steps towards clinical translation. Gene Ther 2009;16:461–9.
[10] Bezencon O, Remen L, Richard S, Roch C, Kessler M, Ertel EA, Moon R, Mawet J, Pfeifer T, Capeleto B. Discovery and evaluation of Cav3.2-selective T-type calcium channel blockers. Bioorg Med Chem Lett 2017;27:5326–31.
[11] Cai S, Gomez K, Moutal A, Khanna R. Targeting T-type/CaV3.2 channels for chronic pain. Transl Res 2021;234:20–30.
[12] Cai W, Zhao Q, Shao J, Zhang J, Li L, Ren X, Su S, Bai Q, Li M, Chen X, Wang J, Cao J, Zang W. MicroRNA-182 alleviates neuropathic pain by regulating Nav1.7 following spared nerve injury in rats. Sci Rep 2018;8:16750.
[13] Campbell JN, Meyer RA. Mechanisms of neuropathic pain. Neuron 2006; 52:77–92.
[14] Catterall WA. Voltage-gated calcium channels. Cold Spring Harb Perspect Biol 2011;3:a003947.
[15] Chemin J, Taiakina V, Monteil A, Piazza M, Guan W, Stephens RF, Kitmitto A, Pang ZP, Dolphin AC, Perez-Reyes E, Dieckmann T, Guillemette JG, Spafford JD. Calmodulin regulates Cav3 T-type channels at their gating brake. J Biol Chem 2017;292:20010–31.
[16] Chen W, Chi YN, Kang XJ, Liu QY, Zhang HL, Li ZH, Zhao ZF, Yang Y, Su L, Cai J, Liao FF, Yi M, Wan Y, Liu FY. Accumulation of Cav3.2 T-type calcium channels in the uninjured sural nerve contributes to neuropathic pain in rats with spared nerve injury. Front Mol Neurosci 2018;11:24.
[17] Choe W, Messinger RB, Leach E, Eckle VS, Obradovic A, Salajegheh R, Jevtovic-Todorovic V, Todorovic SM. TTA-P2 is a potent and selective blocker of T-type calcium channels in rat sensory neurons and a novel antinociceptive agent. Mol Pharmacol 2011;80:900–10.
[18] Chung JM, Chung K. Importance of hyperexcitability of DRG neurons in neuropathic pain. Pain Pract 2002;2:87–97.
[19] Davey NE, Cowan JL, Shields DC, Gibson TJ, Coldwell MJ, Edwards RJ. SLiMPrints: conservation-based discovery of functional motif fingerprints in intrinsically disordered protein regions. Nucleic Acids Res 2012;40:10628–41.
[20] Davey NE, Seo MH, Yadav VK, Jeon J, Nim S, Krystkowiak I, Blikstad C, Dong D, Markova N, Kim PM, Ivarsson Y. Discovery of short linear motif-mediated interactions through phage display of intrinsically disordered regions of the human proteome. FEBS J 2017;284:485–98.
[21] Dudanova I, Sedej S, Ahmad M, Masius H, Sargsyan V, Zhang W, Riedel D, Angenstein F, Schild D, Rupnik M, Missler M. Important contribution of alpha-neurexins to Ca2+-triggered exocytosis of secretory granules. J Neurosci 2006;26:10599–613.
[22] Fan J, Gandini MA, Zhang FX, Chen L, Souza IA, Zamponi GW. Down-regulation of T-type Cav3.2 channels by hyperpolarization-activated cyclic nucleotide-gated channel 1 (HCN1): evidence of a signaling complex. Channels (Austin) 2017;11:434–43.
[23] Finnerup NB, Kuner R, Jensen TS. Neuropathic pain: from mechanisms to treatment. Physiol Rev 2021;101:259–301.
[24] Fischer G, Kostic S, Nakai H, Park F, Sapunar D, Yu H, Hogan Q. Direct injection into the dorsal root ganglion: technical, behavioral, and histological observations. J Neurosci Methods 2011;199:43–55.
[25] Fischer G, Pan B, Vilceanu D, Hogan QH, Yu H. Sustained relief of neuropathic pain by AAV-targeted expression of CBD3 peptide in rat dorsal root ganglion. Gene Ther 2014;21:44–51.
[26] Francois A, Schuetter N, Laffray S, Sanguesa J, Pizzoccaro A, Dubel S, Mantilleri A, Nargeot J, Noel J, Wood JN, Moqrich A, Pongs O, Bourinet E. The low-threshold calcium channel Cav3.2 determines low-threshold mechanoreceptor function. Cell Rep 2015.
[27] Fugere M, Appel J, Houghten RA, Lindberg I, Day R. Short polybasic peptide sequences are potent inhibitors of PC5/6 and PC7: Use of positional scanning-synthetic peptide combinatorial libraries as a tool for the optimization of inhibitory sequences. Mol Pharmacol 2007;71:323–32.
[28] Gadotti VM, Kreitinger JM, Wageling NB, Budke D, Diaz P, Zamponi GW. Cav3.2 T-type calcium channels control acute itch in mice. Mol Brain 2020;13:119.
[29] Garcia-Caballero A, Gadotti VM, Stemkowski P, Weiss N, Souza IA, Hodgkinson V, Bladen C, Chen L, Hamid J, Pizzoccaro A, Deage M, Francois A, Bourinet E, Zamponi GW. The deubiquitinating enzyme USP5 modulates neuropathic and inflammatory pain by enhancing Cav3.2 channel activity. Neuron 2014;83:1144–58.
[30] Garcia-Caballero A, Gandini MA, Huang S, Chen L, Souza IA, Dang YL, Stutts MJ, Zamponi GW. Cav3.2 calcium channel interactions with the epithelial sodium channel ENaC. Mol Brain 2019;12:12.
[31] Gold MS, Gebhart GF. Nociceptor sensitization in pain pathogenesis. Nat Med 2010;16:1248–57.
[32] Gomez K, Calderon-Rivera A, Sandoval A, Gonzalez-Ramirez R, Vargas-Parada A, Ojeda-Alonso J, Granados-Soto V, Delgado-Lezama R, Felix R. Cdk5-Dependent phosphorylation of CaV3.2 T-type channels: possible role in nerve ligation-induced neuropathic allodynia and the compound action potential in primary afferent C fibers. J Neurosci 2020; 40:283–96.
[33] Gonzalez-Perez V, Zeng XH, Henzler-Wildman K, Lingle CJ. Stereospecific binding of a disordered peptide segment mediates BK channel inactivation. Nature 2012;485:133–6.
[34] Huang CH, Chen YC, Chen CC. Physical interaction between calcineurin and Cav3.2 T-type Ca2+ channel modulates their functions. FEBS Lett 2013;587:1723–30.
[35] Huc S, Monteil A, Bidaud I, Barbara G, Chemin J, Lory P. Regulation of T-type calcium channels: signalling pathways and functional implications. Biochim Biophys Acta 2009;1793:947–52.
[36] Hulo N, Bairoch A, Bulliard V, Cerutti L, De Castro E, Langendijk-Genevaux PS, Pagni M, Sigrist CJ. The PROSITE database. Nucleic Acids Res 2006;34:D227–230.
[37] Iakoucheva LM, Radivojac P, Brown CJ, O'Connor TR, Sikes JG, Obradovic Z, Dunker AK. The importance of intrinsic disorder for protein phosphorylation. Nucleic Acids Res 2004;32:1037–49.
[38] Iwaszkiewicz KS, Schneider JJ, Hua S. Targeting peripheral opioid receptors to promote analgesic and anti-inflammatory actions. Front Pharmacol 2013;4:132.
[39] Jacus MO, Uebele VN, Renger JJ, Todorovic SM. Presynaptic Cav3.2 channels regulate excitatory neurotransmission in nociceptive dorsal horn neurons. J Neurosci 2012;32:9374–82.
[40] Joksimovic SL, Joksimovic SM, Tesic V, Garcia-Caballero A, Feseha S, Zamponi GW, Jevtovic-Todorovic V, Todorovic SM. Selective inhibition of CaV3.2 channels reverses hyperexcitability of peripheral nociceptors and alleviates postsurgical pain. Sci Signal 2018;11:eaao4425.
[41] Juarez-Salinas DL, Braz JM, Etlin A, Gee S, Sohal V, Basbaum AI. GABAergic cell transplants in the anterior cingulate cortex reduce neuropathic pain aversiveness. Brain 2019;142:2655–69.
[42] Kerckhove N, Pereira B, Soriot-Thomas S, Alchaar H, Deleens R, Hieng VS, Serra E, Lanteri-Minet M, Arcagni P, Picard P, Lefebvre-Kuntz D, Maindet C, Mick G, Balp L, Lucas C, Creach C, Letellier M, Martinez V, Navez M, Delbrouck D, Kuhn E, Piquet E, Bozzolo E, Brosse C, Lietar B, Marcaillou F, Hamdani A, Leroux-Bromberg N, Perier Y, Vergne-Salle P, Gov C, Delage N, Gillet D, Romettino S, Richard D, Mallet C, Bernard L, Lambert C, Dubray C, Duale C, Eschalier A. Efficacy and safety of a T-type calcium channel blocker in patients with neuropathic pain: a proof-of-concept, randomized, double-blind and controlled trial. Eur J Pain 2018;22:1321–30.
[43] Kerckhove N, Scanzi J, Pereira B, Ardid D, Dapoigny M. Assessment of the effectiveness and safety of ethosuximide in the treatment of abdominal pain related to irritable bowel syndrome - IBSET: protocol of a randomised, parallel, controlled, double-blind and multicentre trial. BMJ Open 2017;7:e015380.
[44] King T, Vera-Portocarrero L, Gutierrez T, Vanderah TW, Dussor G, Lai J, Fields HL, Porreca F. Unmasking the tonic-aversive state in neuropathic pain. Nat Neurosci 2009;12:1364–6.
[45] Kumar M, Gouw M, Michael S, Samano-Sanchez H, Pancsa R, Glavina J, Diakogianni A, Valverde JA, Bukirova D, Calyseva J, Palopoli N, Davey NE, Chemes LB, Gibson TJ. ELM-the eukaryotic linear motif resource in 2020. Nucleic Acids Res 2020;48:D296–306.
[46] LeBlanc BW, Lii TR, Huang JJ, Chao YC, Bowary PM, Cross BS, Lee MS, Vera-Portocarrero LP, Saab CY. T-type calcium channel blocker Z944 restores cortical synchrony and thalamocortical connectivity in a rat model of neuropathic pain. PAIN 2016;157:255–63.
[47] Lee S. Pharmacological inhibition of voltage-gated Ca(2+) channels for chronic pain relief. Curr Neuropharmacol 2013;11:606–20.
[48] Lory P, Nicole S, Monteil A. Neuronal Cav3 channelopathies: recent progress and perspectives. Pflugers Arch 2020;472:831–44.
[49] Madeira F, Park YM, Lee J, Buso N, Gur T, Madhusoodanan N, Basutkar P, Tivey ARN, Potter SC, Finn RD, Lopez R. The EMBL-EBI search and sequence analysis tools APIs in 2019. Nucleic Acids Res 2019;47:W636–41.

[50] Martinez-Hernandez E, Zeglin A, Almazan E, Perissinotti P, He Y, Koob M, Martin JL, Piedras-Renteria ES. KLHL1 controls CaV3.2 expression in DRG neurons and mechanical sensitivity to pain. Front Mol Neurosci 2019;12:315.
[51] Mason MR, Ehlert EM, Eggers R, Pool CW, Hermening S, Huseinovic A, Timmermans E, Blits B, Verhaagen J. Comparison of AAV serotypes for gene delivery to dorsal root ganglion neurons. Mol Ther 2010;18:715–24.
[52] Messinger RB, Naik AK, Jagodic MM, Nelson MT, Lee WY, Choe WJ, Orestes P, Latham JR, Todorovic SM, Jevtovic-Todorovic V. In vivo silencing of the Ca(V)3.2 T-type calcium channels in sensory neurons alleviates hyperalgesia in rats with streptozocin-induced diabetic neuropathy. PAIN 2009;145:184–95.
[53] Mogil JS. Sex differences in pain and pain inhibition: multiple explanations of a controversial phenomenon. Nat Rev Neurosci 2012;13:859–66.
[54] Monteil A, Chausson P, Boutourlinsky K, Mezghrani A, Huc-Brandt S, Blesneac I, Bidaud I, Lemmers C, Leresche N, Lambert RC, Lory P. Inhibition of Cav3.2 T-type calcium channels by its intracellular I-II loop. J Biol Chem 2015;290:16168–76.
[55] Montera M, Goins A, Cmarko L, Weiss N, Westlund KN, Alles SRA. Trigeminal neuropathic pain is alleviated by inhibition of Cav3.3 T-type calcium channels in mice. Channels (Austin) 2021;15:31–7.
[56] Na HS, Choi S, Kim J, Park J, Shin HS. Attenuated neuropathic pain in Cav3.1 null mice. Mol Cells 2008;25:242–6.
[57] Nelson MT, Joksovic PM, Perez-Reyes E, Todorovic SM. The endogenous redox agent L-cysteine induces T-type Ca2+ channel-dependent sensitization of a novel subpopulation of rat peripheral nociceptors. J Neurosci 2005;25:8766–75.
[58] O'Brien KT, Golla K, Kranjc T, O'Donovan D, Allen S, Maguire P, Simpson JC, O'Connell D, Moran N, Shields DC. Computational and experimental analysis of bioactive peptide linear motifs in the integrin adhesome. PLoS One 2019;14:e0210337.
[59] Pan B, Guo Y, Wu HE, Park J, Trinh VN, Luo ZD, Hogan QH. Thrombospondin-4 divergently regulates voltage-gated Ca2+ channel subtypes in sensory neurons after nerve injury. PAIN 2016;157:2068–80.
[60] Pan B, Yu H, Fischer GJ, Kramer JM, Hogan QH. Dorsal root ganglionic field stimulation relieves spontaneous and induced neuropathic pain in rats. J Pain 2016;17:1349–58.
[61] Pan B, Yu H, Park J, Yu YP, Luo ZD, Hogan QH. Painful nerve injury upregulates thrombospondin-4 expression in dorsal root ganglia. J Neurosci Res 2015;93:443–53.
[62] Park HJ, Sandor K, McQueen J, Woller SA, Svensson CI, Corr M, Yaksh TL. The effect of gabapentin and ketorolac on allodynia and conditioned place preference in antibody-induced inflammation. Eur J Pain 2016;20:917–25.
[63] Patel R, Montagut-Bordas C, Dickenson AH. Calcium channel modulation as a target in chronic pain control. Br J Pharmacol 2018;175:2173–84.
[64] Perez-Reyes EG. protein-mediated inhibition of Cav3.2 T-type channels revisited. Mol Pharmacol 2010;77:136–8.
[65] Pfirrmann CW, Oberholzer PA, Zanetti M, Boos N, Trudell DJ, Resnick D, Hodler J. Selective nerve root blocks for the treatment of sciatica: evaluation of injection site and effectiveness—a study with patients and cadavers. Radiology 2001;221:704–11.
[66] Pleticha J, Heilmann LF, Evans CH, Asokan A, Samulski RJ, Beutler AS. Preclinical toxicity evaluation of AAV for pain: evidence from human AAV studies and from the pharmacology of analgesic drugs. Mol Pain 2014;10:54.
[67] Pleticha J, Maus TP, Beutler AS. Future directions in pain management: integrating anatomically selective delivery techniques with novel molecularly selective agents. Mayo Clin Proc 2016;91:522–33.
[68] Pleticha J, Maus TP, Christner JA, Marsh MP, Lee KH, Hooten WM, Beutler AS. Minimally invasive convection-enhanced delivery of biologics into dorsal root ganglia: validation in the pig model and prospective modeling in humans. Technical note. J Neurosurg 2014;121:851–8.
[69] Raja SN, Ringkamp M, Guan Y, Campbell JN. John J. Bonica Award Lecture: peripheral neuronal hyperexcitability: the "low-hanging" target for safe therapeutic strategies in neuropathic pain. PAIN 2020;161(suppl 1):S14–26.
[70] Rehak R, Bartoletti TM, Engbers JD, Berecki G, Turner RW, Zamponi GW. Low voltage activation of KCa1.1 current by Cav3-KCa1.1 complexes. PLoS One 2013;8:e61844.
[71] Rickman C, Archer DA, Meunier FA, Craxton M, Fukuda M, Burgoyne RD, Davletov B. Synaptotagmin interaction with the syntaxin/SNAP-25 dimer is mediated by an evolutionarily conserved motif and is sensitive to inositol hexakisphosphate. J Biol Chem 2004;279:12574–9.
[72] Roberts-Crowley ML, Mitra-Ganguli T, Liu L, Rittenhouse AR. Regulation of voltage-gated Ca2+ channels by lipids. Cell Calcium 2009;45:589–601.
[73] Roy A, Kucukural A, Zhang Y. I-TASSER: a unified platform for automated protein structure and function prediction. Nat Protoc 2010;5:725–38.
[74] Rzhepetskyy Y, Lazniewska J, Proft J, Campiglio M, Flucher BE, Weiss N. A Cav3.2/Stac1 molecular complex controls T-type channel expression at the plasma membrane. Channels (Austin) 2016;10:346–54.
[75] Shen FY, Chen ZY, Zhong W, Ma LQ, Chen C, Yang ZJ, Xie WL, Wang YW. Alleviation of neuropathic pain by regulating T-type calcium channels in rat anterior cingulate cortex. Mol Pain 2015;11:7.
[76] Shin SM, Cai Y, Itson-Zoske B, Qiu C, Hao X, Xiang H, Hogan QH, Yu H. Enhanced T-type calcium channel 3.2 activity in sensory neurons contributes to neuropathic-like pain of monosodium iodoacetate-induced knee osteoarthritis. Mol Pain 2020;16:1744806920963807.
[77] Shin SM, Itson-Zoske B, Cai Y, Qiu C, Pan B, Stucky CL, Hogan QH, Yu H. Satellite glial cells in sensory ganglia express functional transient receptor potential ankyrin 1 that is sensitized in neuropathic and inflammatory pain. Mol Pain 2020;16:1744806920925425.
[78] Shin SM, Wang F, Qiu C, Itson-Zoske B, Hogan QH, Yu H. Sigma-1 receptor activity in primary sensory neurons is a critical driver of neuropathic pain. Gene Ther 2022;29:1–15.
[79] Snutch TP, Zamponi GW. Recent advances in the development of T-type calcium channel blockers for pain intervention. Br J Pharmacol 2018;175:2375–83.
[80] Tomita S, Sekiguchi F, Deguchi T, Miyazaki T, Ikeda Y, Tsubota M, Yoshida S, Nguyen HD, Okada T, Toyooka N, Kawabata A. Critical role of Cav3.2 T-type calcium channels in the peripheral neuropathy induced by bortezomib, a proteasome-inhibiting chemotherapeutic agent, in mice. Toxicology 2018;413:33–9.
[81] Wallace M, Duan R, Liu W, Locke C, Nothaft W. A randomized, double-blind, placebo-controlled, crossover study of the T-type calcium channel blocker ABT-639 in an intradermal capsaicin experimental pain model in healthy adults. Pain Med 2016;17:551–60.
[82] Watanabe M, Ueda T, Shibata Y, Kumamoto N, Shimada S, Ugawa S. Expression and regulation of Cav3.2 T-type calcium channels during inflammatory hyperalgesia in mouse dorsal root ganglion neurons. PLoS One 2015;10:e0127572.
[83] Weiss N, Hameed S, Fernandez-Fernandez JM, Fablet K, Karmazinova M, Poillot C, Proft J, Chen L, Bidaud I, Monteil A, Huc-Brandt S, Lacinova L, Lory P, Zamponi GW, De Waard M. A Ca(v)3.2/syntaxin-1A signaling complex controls T-type channel activity and low-threshold exocytosis. J Biol Chem 2012;287:2810–18.
[84] Woolf CJ. Overcoming obstacles to developing new analgesics. Nat Med 2010;16:1241–7.
[85] Woolf CJ. Capturing novel non-opioid pain targets. Biol Psychiatry 2020;87:74–81.
[86] Wright PE, Dyson HJ. Intrinsically disordered proteins in cellular signalling and regulation. Nat Rev Mol Cell Biol 2015;16:18–29.
[87] Xiang H, Liu Z, Wang F, Xu H, Roberts C, Fischer G, Stucky C, Caron D, Pan B, Hogan Q, Yu H. Primary sensory neuron-specific interference of TRPV1 signaling by AAV-encoded TRPV1 peptide aptamer attenuates neuropathic pain. Mol Pain 2017;13:1744806917717040.
[88] Xue B, Dunbrack RL, Williams RW, Dunker AK, Uversky VN. PONDR-FIT: a meta-predictor of intrinsically disordered amino acids. Biochim Biophys Acta 2010;1804:996–1010.
[89] Yekkirala AS, Roberson DP, Bean BP, Woolf CJ. Breaking barriers to novel analgesic drug development. Nat Rev Drug Discov 2017;16:810.
[90] Yu H, Fischer G, Ferhatovic L, Fan F, Light AR, Weihrauch D, Sapunar D, Nakai H, Park F, Hogan QH. Intraganglionic AAV6 results in efficient and long-term gene transfer to peripheral sensory nervous system in adult rats. PloS one 2013;8:e61266.
[91] Yu H, Fischer G, Jia G, Reiser J, Park F, Hogan QH. Lentiviral gene transfer into the dorsal root ganglion of adult rats. Mol Pain 2011;7:63.
[92] Yu H, Pan B, Weyer A, Wu HE, Meng J, Fischer G, Vilceanu D, Light AR, Stucky C, Rice FL, Hudmon A, Hogan Q. CaMKII controls whether touch is painful. J Neurosci 2015;35:14086–102.
[93] Yu H, Shin SM, Xiang H, Chao D, Cai Y, Xu H, Khanna R, Pan B, Hogan QH. AAV-encoded CaV2.2 peptide aptamer CBD3A6K for primary sensory neuron-targeted treatment of established neuropathic pain. Gene Ther 2019;26:308–23.
[94] Zarin T, Tsai CN, Nguyen Ba AN, Moses AM. Selection maintains signaling function of a highly diverged intrinsically disordered region. Proc Natl Acad Sci U S A 2017;114:E1450–9.
[95] Zhang B, Gao Y, Moon SY, Zhang Y, Zheng Y. Oligomerization of Rac1 gtpase mediated by the carboxyl-terminal polybasic domain. J Biol Chem 2001;276:8958–67.
[96] Zhou J, Oldfield CJ, Yan W, Shen B, Dunker AK. Intrinsically disordered domains: sequence disorder function relationships. Protein Sci 2019;28:1652–63.
[97] Zhou L, Middel V, Reischl M, Strahle U, Nienhaus GU. Distinct amino acid motifs carrying multiple positive charges regulate membrane targeting of dysferlin and MG53. PLoS One 2018;13:e0202052.
[98] Ziegler D, Duan WR, An G, Thomas JW, Nothaft W. A randomized double-blind, placebo-, and active-controlled study of T-type calcium channel blocker ABT-639 in patients with diabetic peripheral neuropathic pain. PAIN 2015;156:2013–20.